For presentation at the US-Canada Fuel Cell Workshop, Institute for Fuel Cell Innovation, National Research Council, 4250 Wesbrook Mall, Vancouver, BC, March 17 – 18, 2008.

SAND2008-1689C

Elucidating Water Transport and Removal in PEM Fuel Cells via Experiments and Modeling

Ken S. Chen* and Mike A. Hickner**

*** Engineering Sciences Center**
Sandia National Laboratories, Albuquerque, NM87185

**** Presently at: Department of Materials Science & Engineering**
The Pennsylvania State University, University Park, PA 16802

Collaborators:

Nathan Siegel (SNL)
David Noble (SNL)

Prof. Chao-Yang Wang and research associates (ECEC/PSU)
Prof. Ugur Pasaogullari (ECEC/PSU, presently UConn at Storr)

Sandia National Laboratories

Motivation

- PEM (Proton Exchange Membrane) fuel cells are becoming an important energy conversion technology for automotive & stationary applications.
- Water removal is critical to maintaining PEM fuel cell performance and durability.
- If the water is not removed effectively, excessive water will accumulate leading to “flooding”, which prevents oxygen from reaching the reaction sites.
- The water removal issue has not gotten much attention previously because most researchers have focused on the electrochemical aspects of PEM fuel cells.
- Water transport is a technically challenging problem to address:
  - Small scale makes direct observations difficult.
  - Electrochemical nature limits the choice of experimental techniques.
  - Complex, coupled transport phenomena adds to the technical challenges.

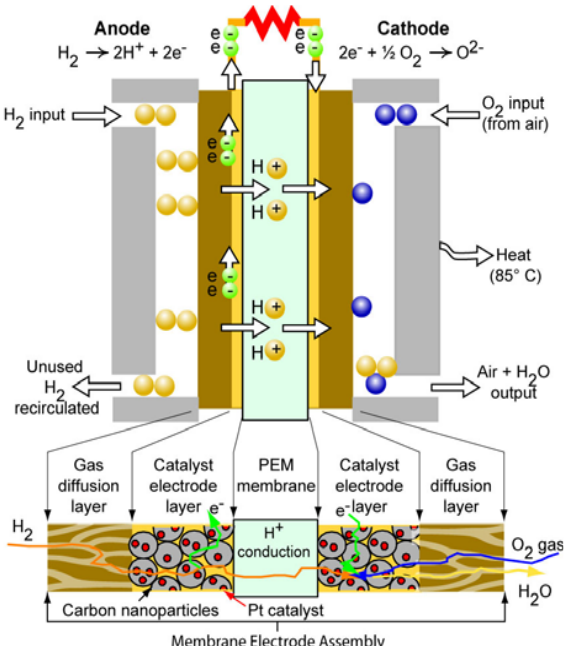

• We employ both experimental techniques and computational models for addressing this emerging and critical area of water removal in PEM fuel cells.

Sandia National Laboratories

Water transport & removal in PEM fuel cells

Source for Diagram:
U. Pasaogullari and C.-Y. Wang (2003, 2004)

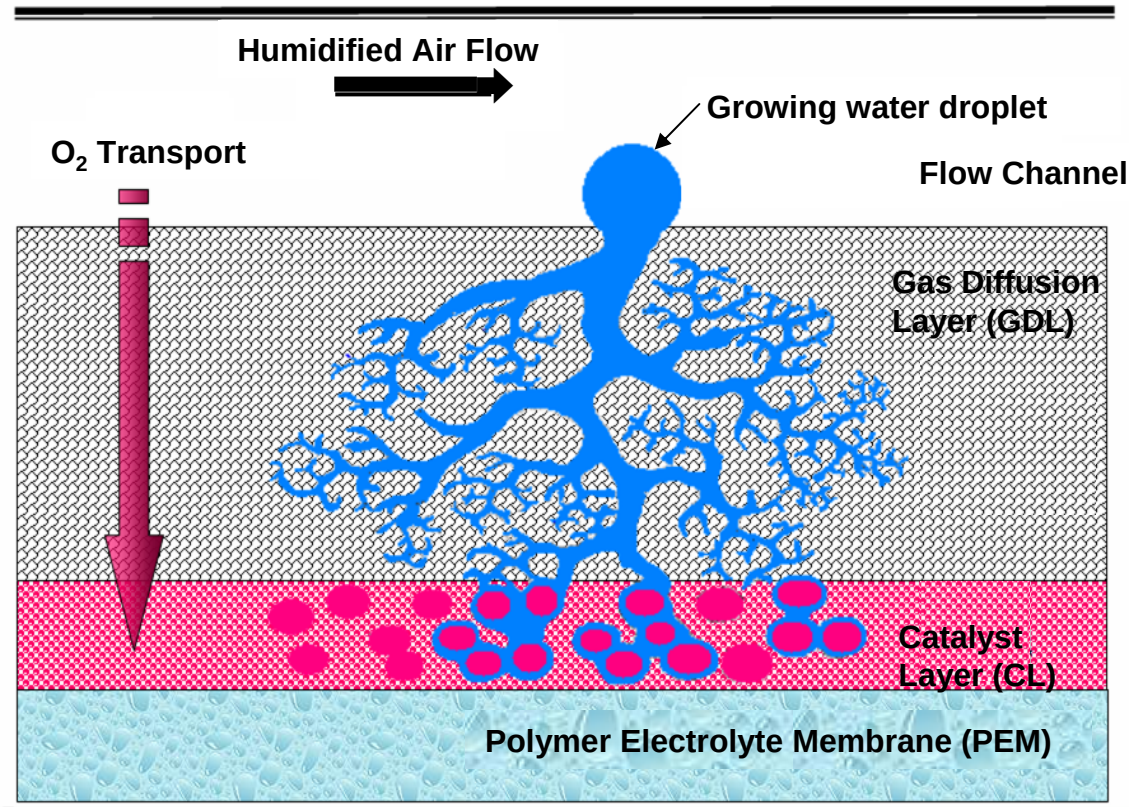

- **Water generated in the CL via the oxygen oxidation reaction.**
- **Water vapor can condense to liquid water within the CL and GDL.**
- **Liquid water is transported within the CL and GDL via capillary action.**
- **Water droplet can form and grow at the GDL/channel interface.**
- **Water droplet can be deformed and detached at the GDL/channel interface via shear force and pressure drag.**

Sandia National Laboratories

Probing liquid-water distribution using the state-of-the-art neutron imaging facility at NIST

Collaborators:
Dan Hussey
David Jacobson
Muhammad Arif

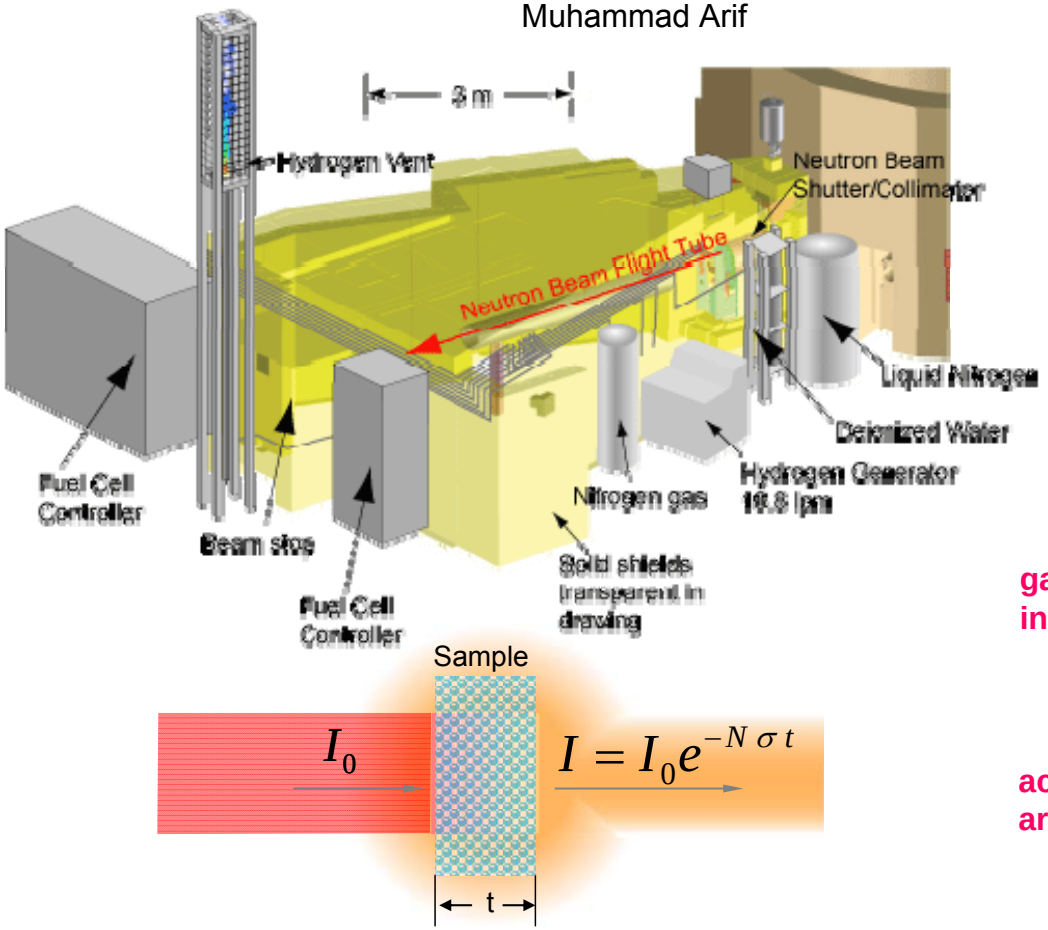

I_0 – *incident intensity,* I – *transmitted intensity,*

Active area of fuel cell generates water

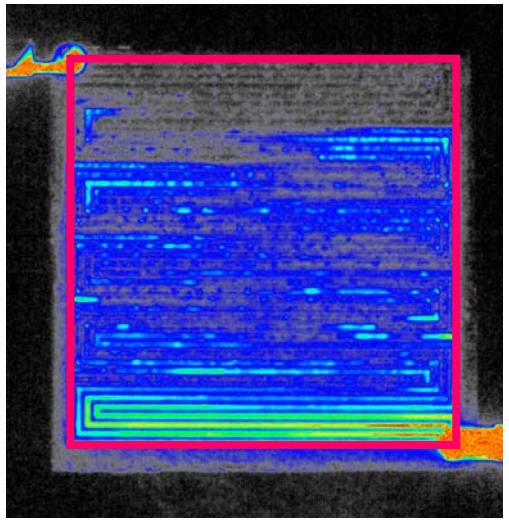

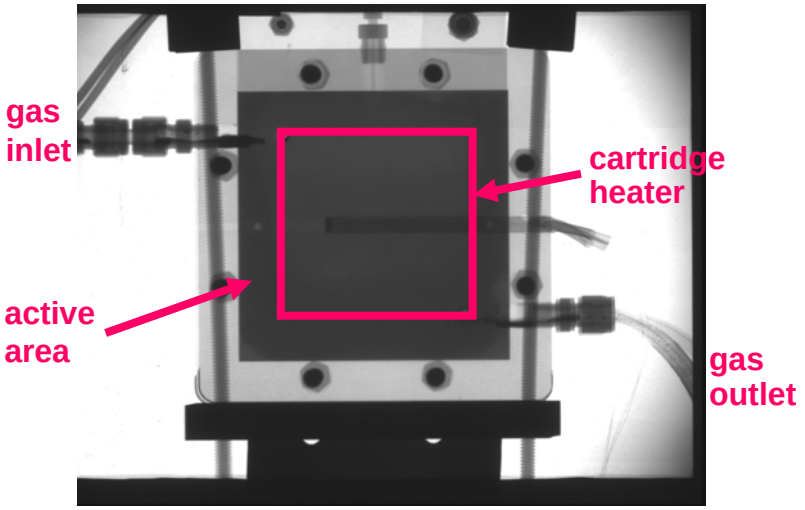

Sandia National Laboratories

50 cm² cell, Quad serpentine flow channel, H_2/Air coflow, 1 Hz sampling, 130 μm spacial resolution.

Effect of current density on liquid-water content – 40°C

(Operating conditions: 40°C, 2 stoic, 50 kPa)

0 A/cm²

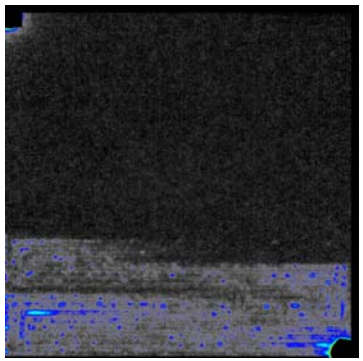

3.4 mg/cm² H_2O

0.1 A/cm2

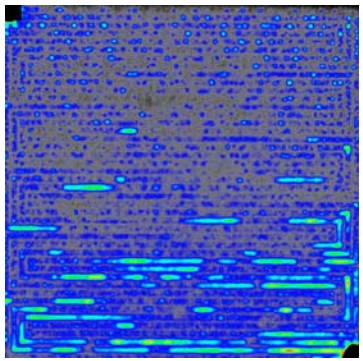

13.8 mg/cm2 H_2O

0.25 A/cm2

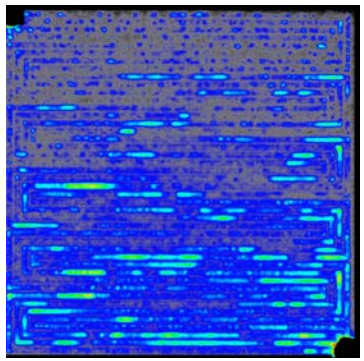

15.6 mg/cm2 H_2O

0.5 A/cm2

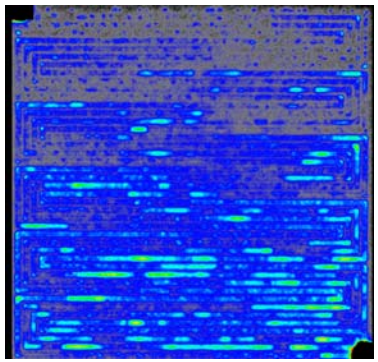

16.4 mg/cm2 H_2O

0.75 A/cm²

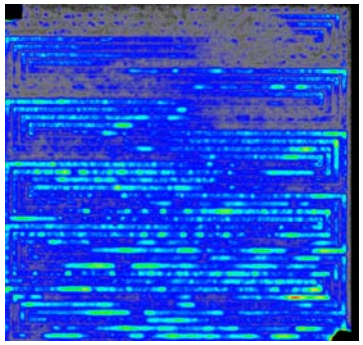

18.4 mg/cm2 H_2O

1.0 A/cm²

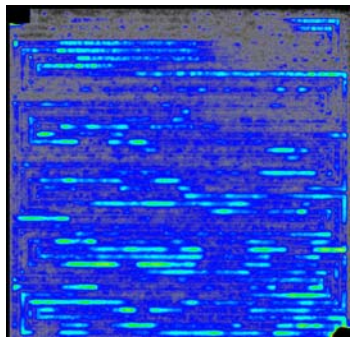

16.0 mg/cm2 H_2O

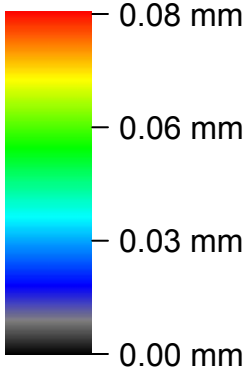

High water concentration

Low water concentration

- **Liquid-water content arises with increasing current density, up to a certain point.**

Sandia National Laboratories

Reference: M. A. Hickner, N. P. Siegel, K. S. Chen, D. S. Hussey, D. L. Jacobson and M. Arif, J. Electrochem. Soc., 155 (3) B294 – B302 (2008).

Effect of current density on liquid-water content – 60°C

(Operating conditions: 60°C, 2 stoic, 50 kPa)

0 A/cm²

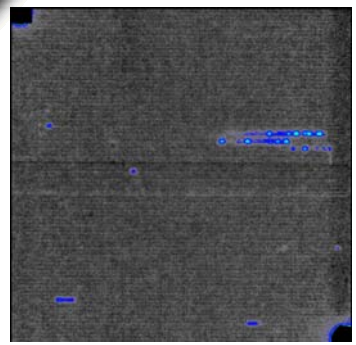

5.0 mg/cm² H_2O

0.1 A/cm2

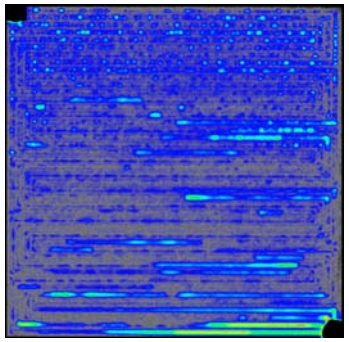

14.2 mg/cm² H_2O

0.25 A/cm2

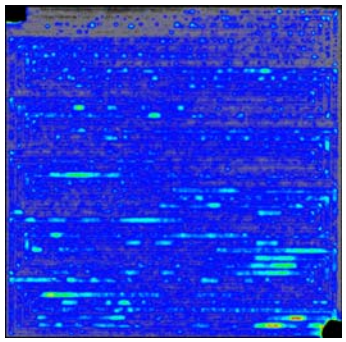

16.4 mg/cm² H_2O

0.5 A/cm2

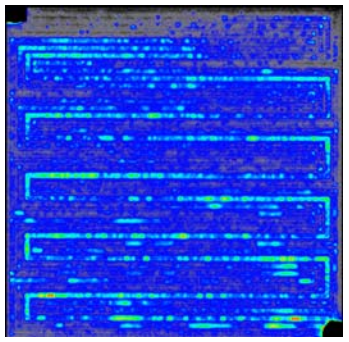

17.6 mg/cm² H_2O

0.75 A/cm²

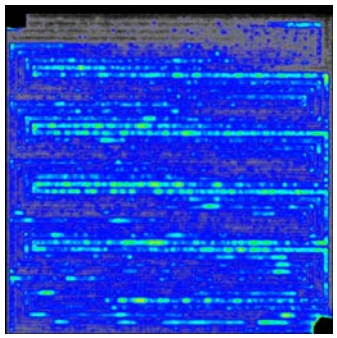

17.8 mg/cm² H_2O

1.0 A/cm²

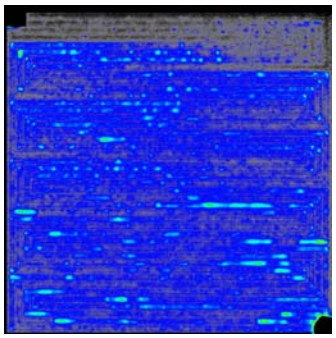

15.0 mg/cm² H_2O

1.25A A/cm²

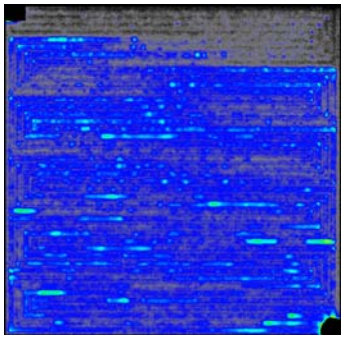

14.6 mg/cm² H_2O

1.50 A/cm²

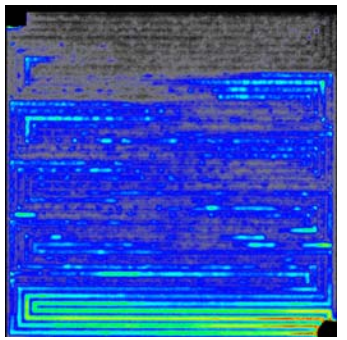

16.6 mg/cm² H_2O

- **Liquid-water content arises with increasing current density, upto a certain point.**
- **Liquid-water content is lower at 60°C than at 40°C, as expected.**

Effect of current density on liquid-water content – 80ºC

(Operating conditions: 80°C, 2 stoic, 50 kPa)

0 A/cm²

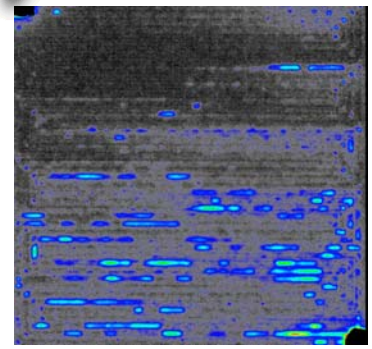

0.411 mL H_2O

0.1 A/cm2

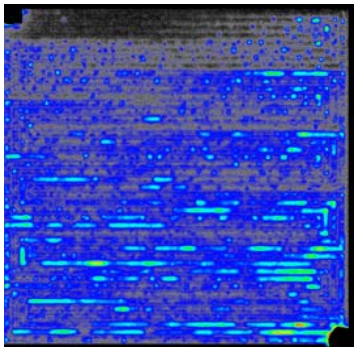

0.714 mL H_2O

0.25 A/cm2

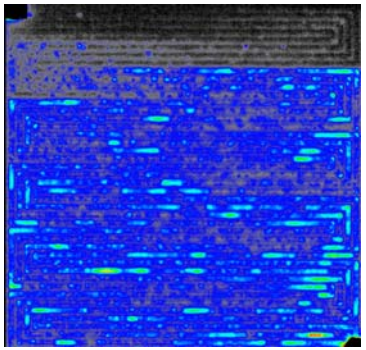

0.734 mL H_2O

0.5 A/cm2

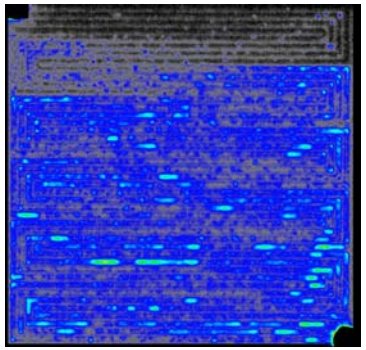

0.664 mL H_2O

0.75 A/cm²

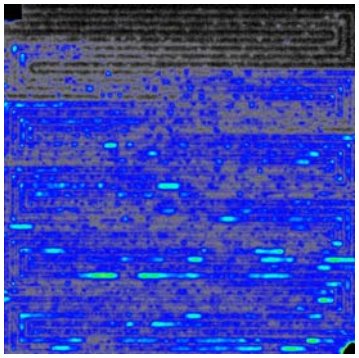

0.614 mL H_2O

1.0 A/cm²

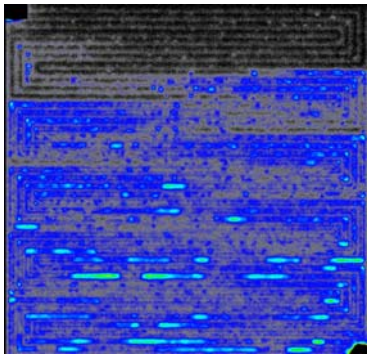

0.571 mL H_2O

1.25A A/cm²

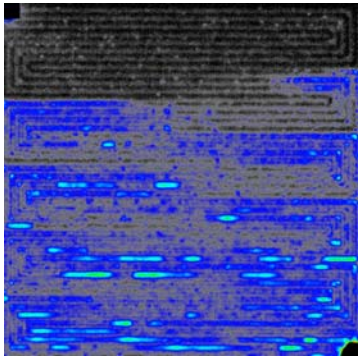

0.510 mL H_2O

1.50 A/cm²

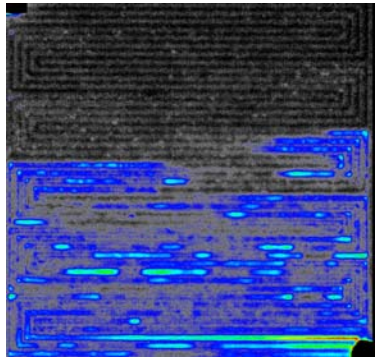

0.453 mL H_2O

- **Liquid-water content arises with increasing current density, upto a certain point.**
- **Liquid-water content is lower at 80ºC than at 60ºC and 40ºC, as expected.**

Dynamic liquid water distribution inside a PEMFC's active area was successfully monitored in real time

Liquid water accumulates rapidly when current load is applied, but drains slowly when the load is ceased.

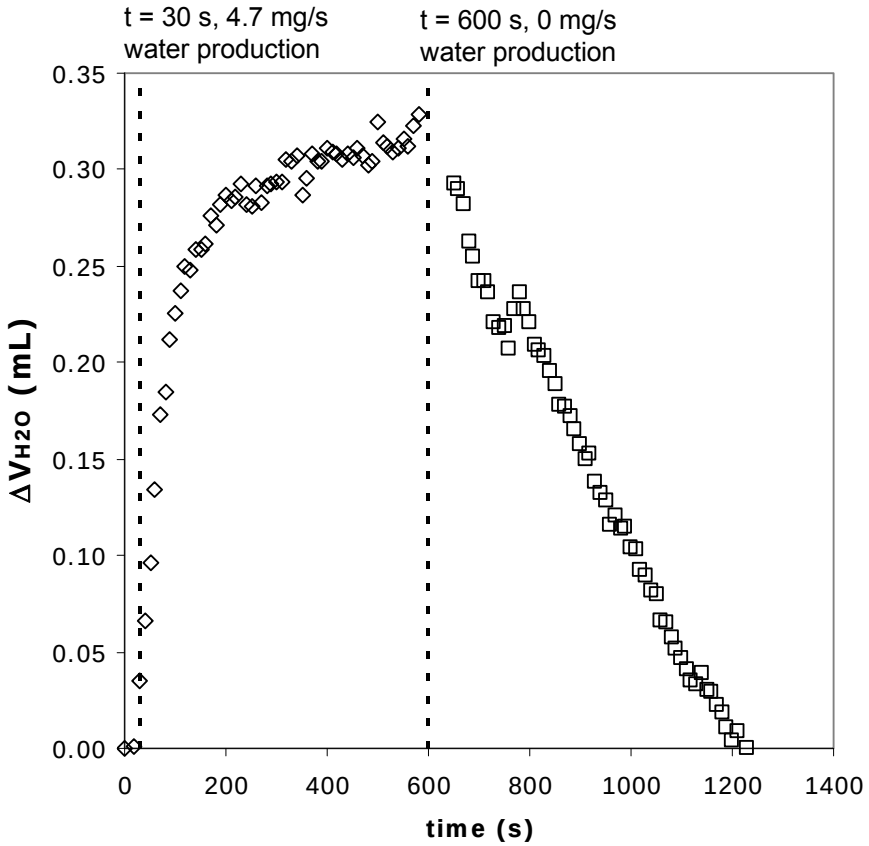

Operating conditions: 40°C
0 mA/cm^2 → 1000 mA/cm^2 → 0 mA/cm^2

This movie clip shows some of the clearest images of liquid water distribution obtained to date! These images provide insights for developing water transport models.

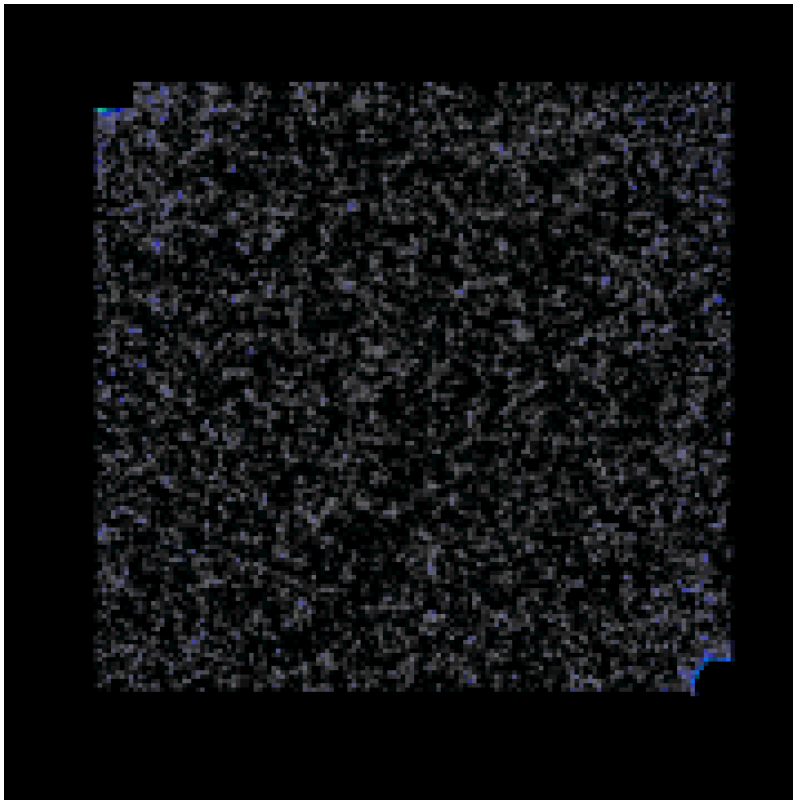

Operating conditions: 80°C, 0 mA/cm^2 → 1500 mA/cm^2
10 min. compressed

Sandia National Laboratories

Where is the water?

anode – membrane – cathode

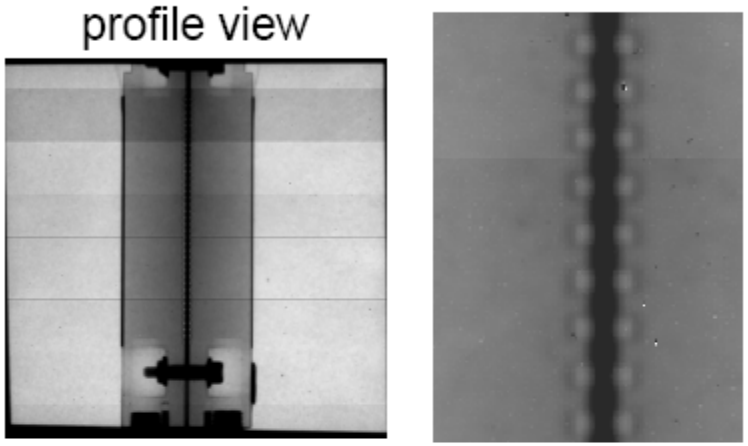

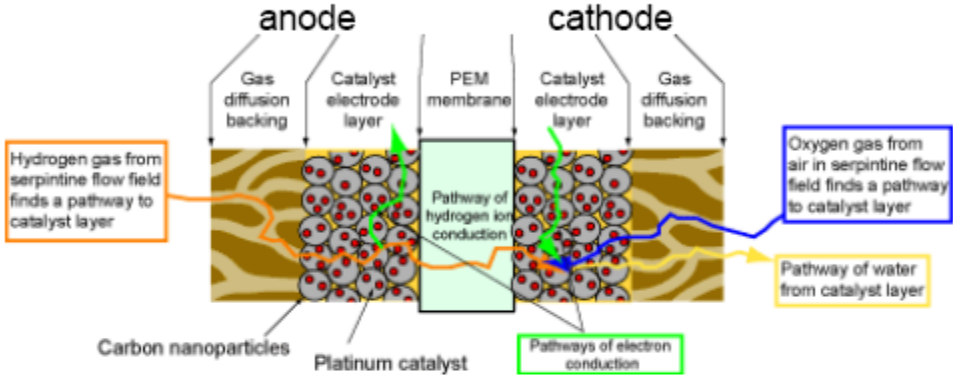

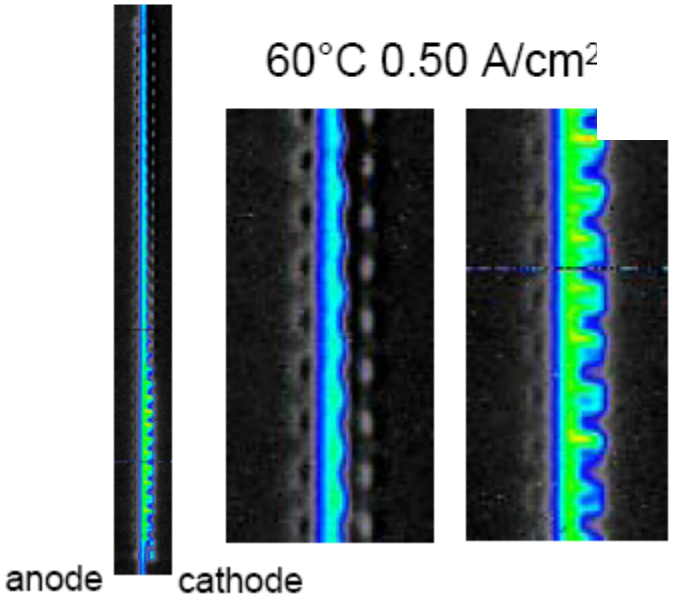

Highted liquid water content across MEA (60 °C, 0.5 A/cm^2)

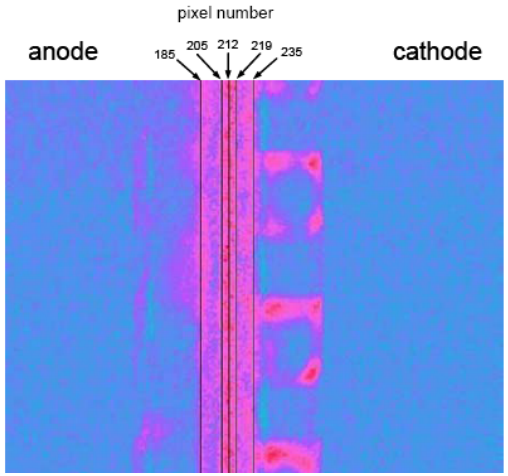

Ref.: M. A. Hickner, N. P. Siegel, K. S. Chen, D. S. Hussey, D. L. Jacobson, M. Arif, *JES*, 155, B427 (2008).

Liquid water distribution across the MEA

(Operating conditions: 60°C, 2 stoic,100% RH)

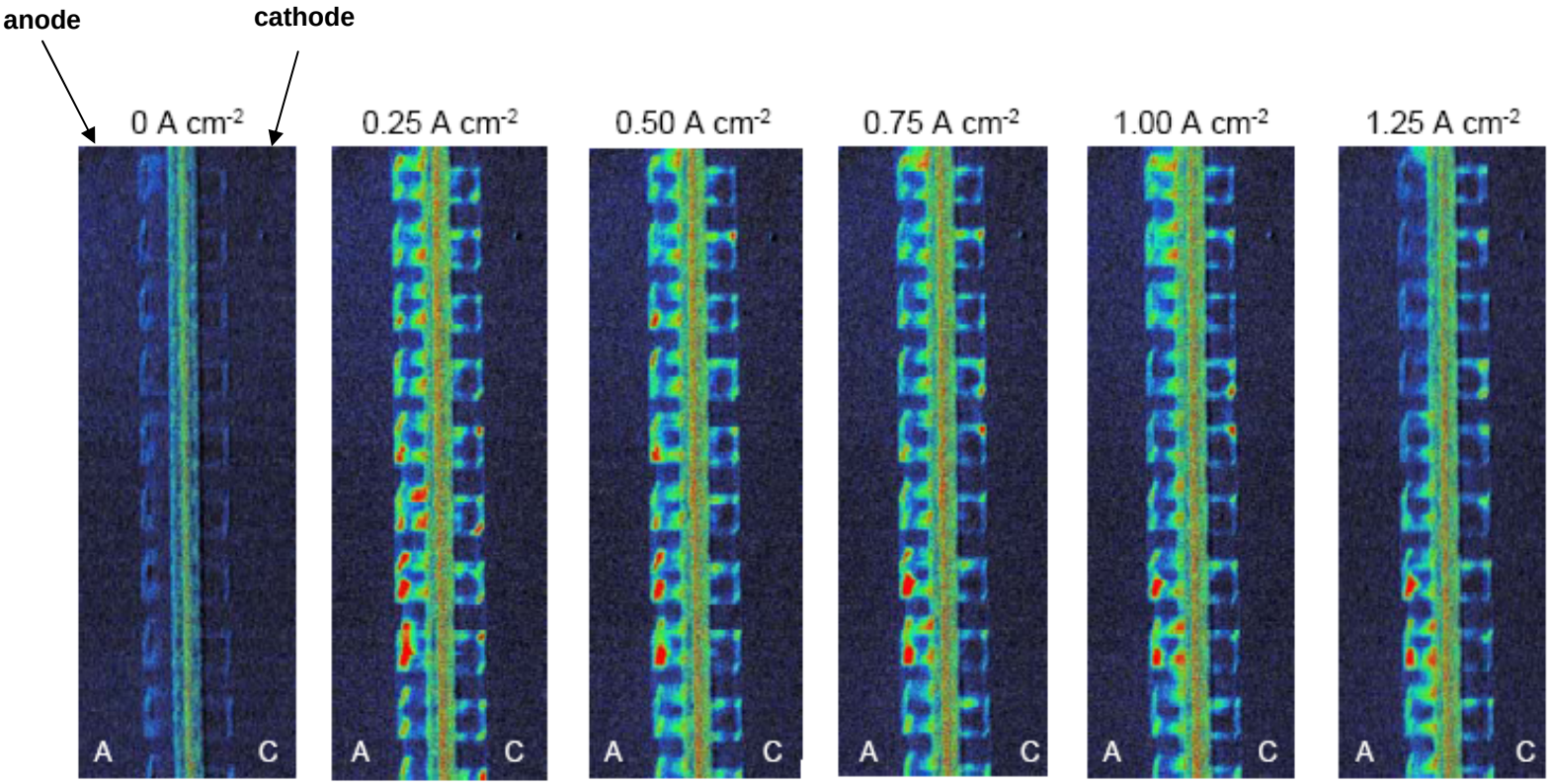

Effects of temperature and current density on liquid water distribution across MEA

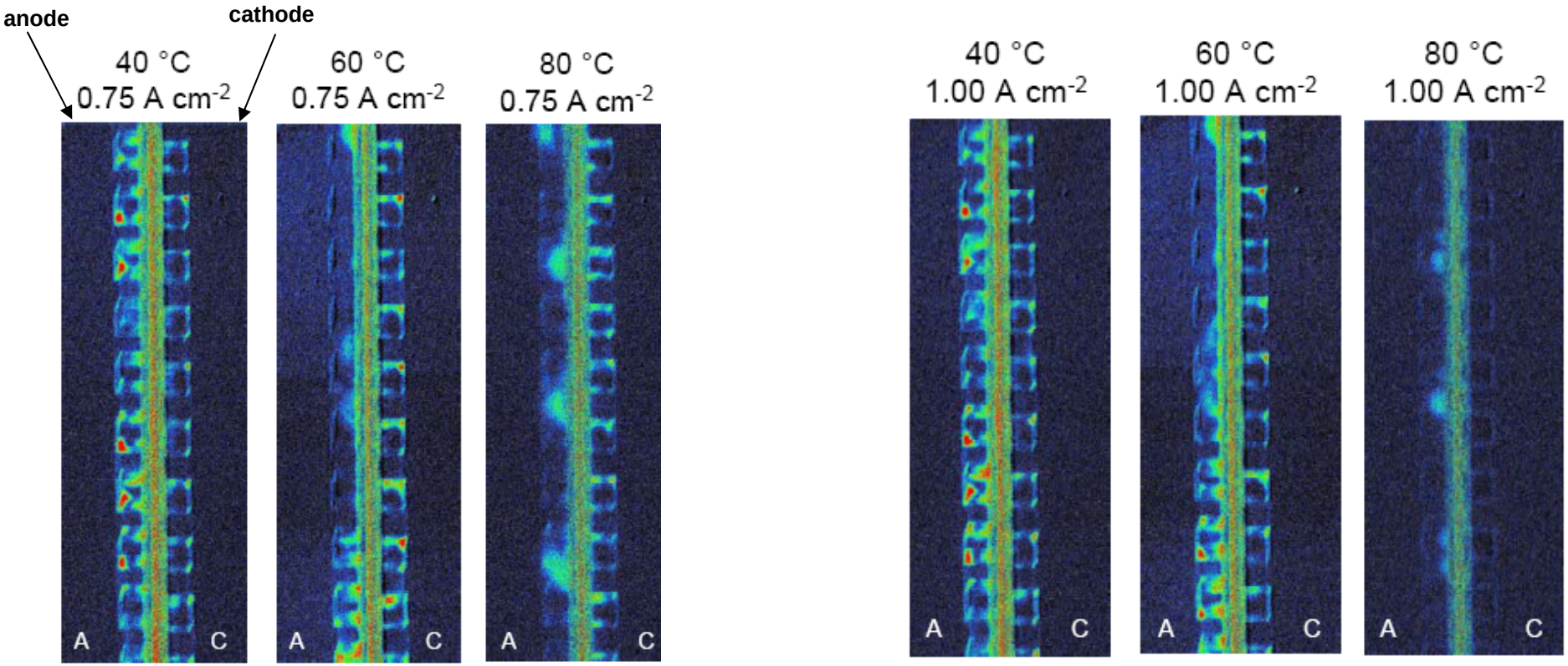

Effects of stoichiometric flow ratio and current density on liquid water distribution across MEA (60 °C, 100% RH)

Current density = 0.5 A/cm^2

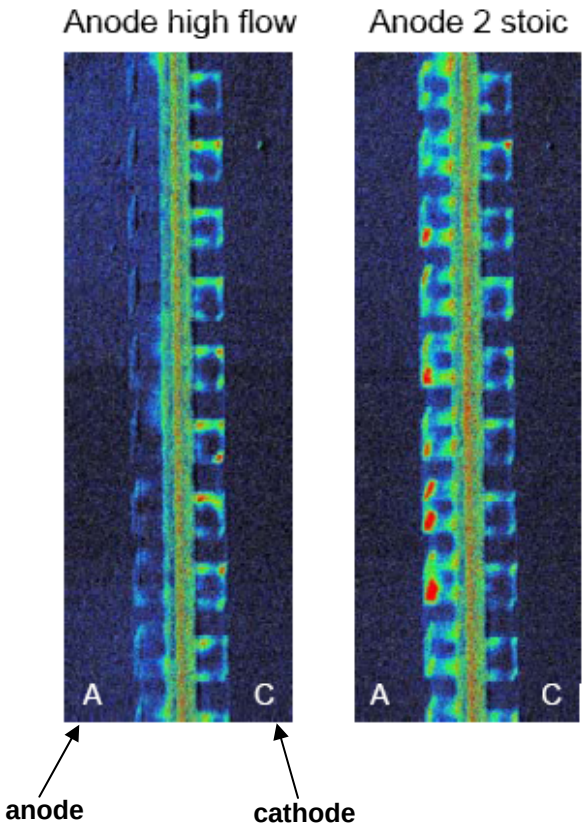

Current density = 1.0 A/cm^2

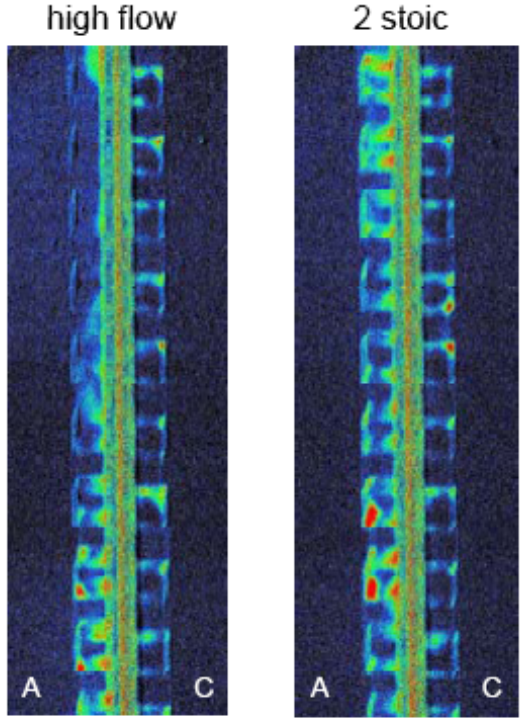

Visualization of water-droplet growth and removal at GDL/channel interface

Transparent fuel cell visualization apparatus

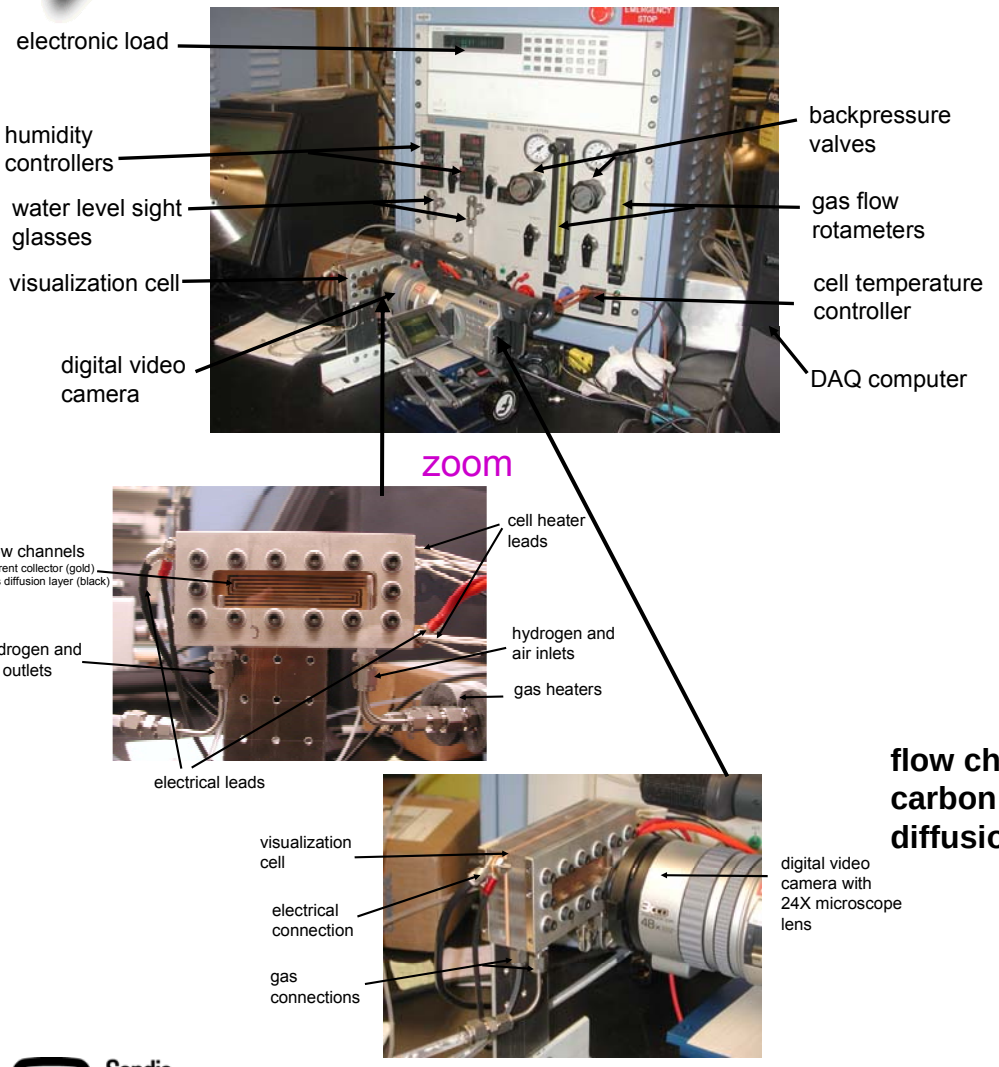

Sample image of two liquid-water droplets

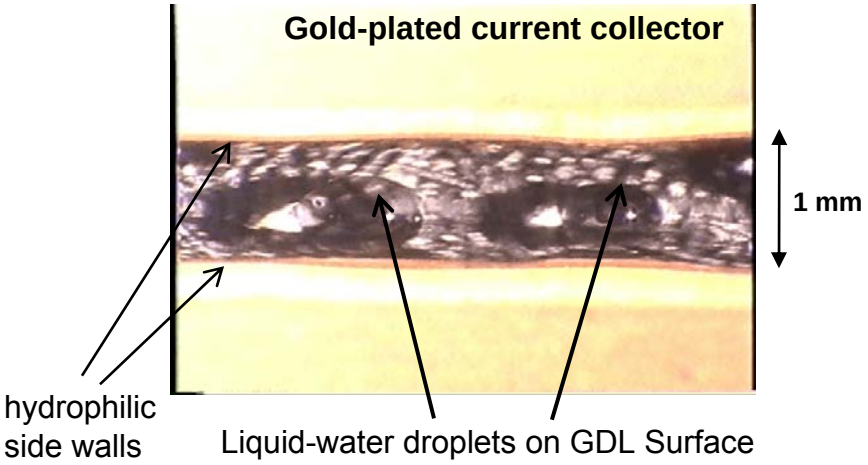

Droplet formation and growth near side wall

flow channel with carbon paper gas diffusion layer

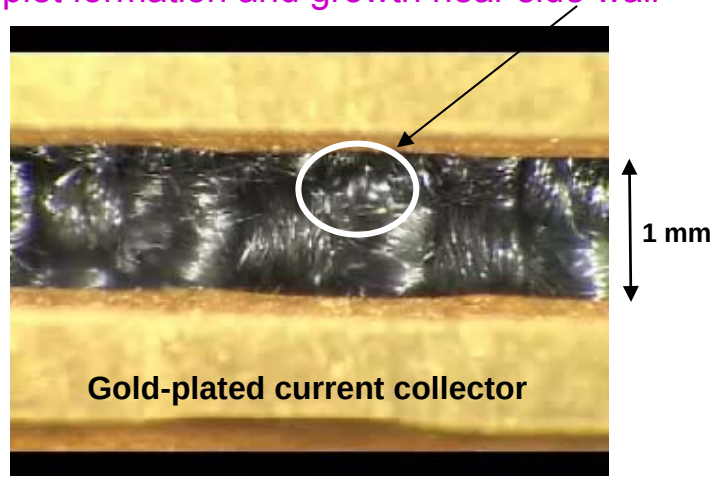

Sandia National Laboratories

Collaborators: Mike Hickner (Penn State U., formerly SNL), C.-Y. Wang (PSU)

Visualizing water-droplet dynamic behavior in a simulated cathode – experimental apparatus

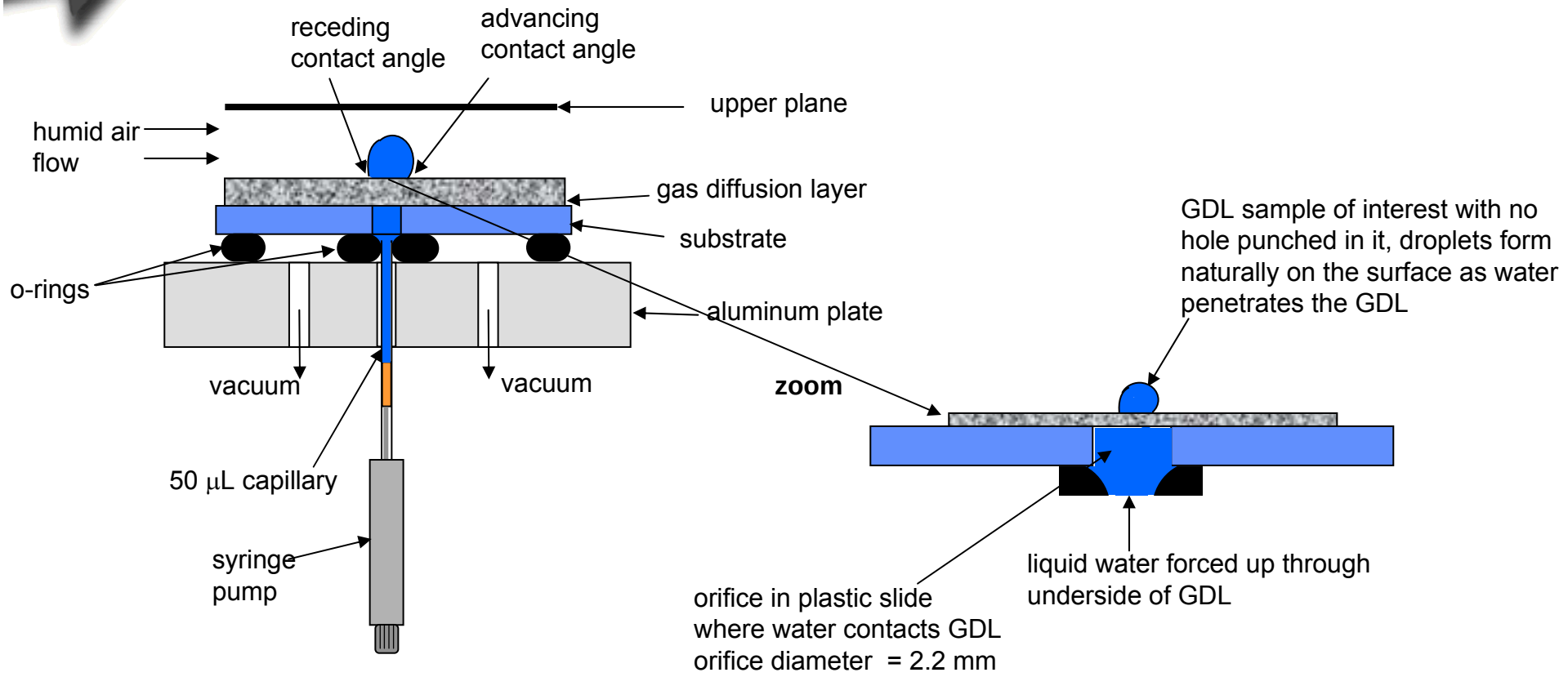

- **Contact-angle hysteresis (θ_a-θ_r) at GDL/flow-channel interface depends on**
  - **-- wetting properties, surface roughness of GDL/flow-channel interface**
  - **-- geometry and flow condition in the air-flow channel**
  - **-- liquid-water generation rate (which depends on cell current density)**
  - **-- pore structure and hydrophobic/hydrophilic nature of GDL**

Sandia National Laboratories

Reference: Chen, Hickner and Noble , *Int. J. Energy Research*, Vol. 29 (2005)

Droplet growth and contact-angle hysteresis measurements

(Parameters: air flow velocity ~ 750 cm/s, Q_{water} ~ 1 μL/min, treated Toray GDL)

H – droplet height, 2B – flow channel height = 2 mm.

t = 0, H/2B = 0.29
θ_a = 88°, θ_r = 70°, (θ_a-θ_r) = 18°

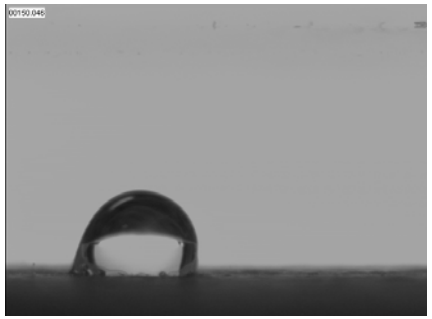

t = 20 seconds, H/2B = 0.5
θ_a = 120°, θ_r = 80°, (θ_a-θ_r) = 40°

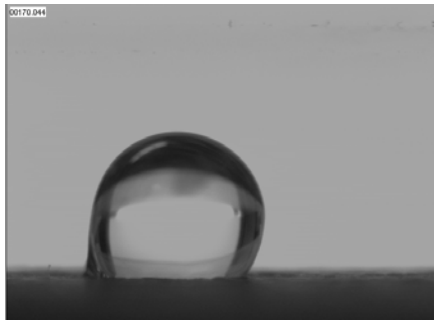

t = 40 seconds, H/2B = 0.59
θ_a = 123°, θ_r = 78°, (θ_a-θ_r) = 45°

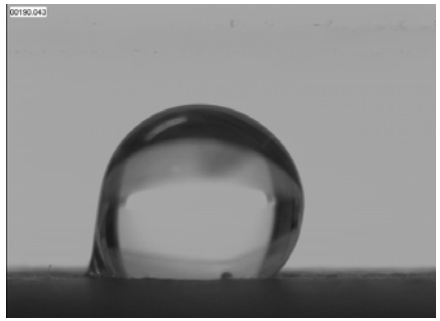

t = 65 seconds, H/2B = 0.65
θ_a = 128°, θ_r = 77°, (θ_a-θ_r) = 51°

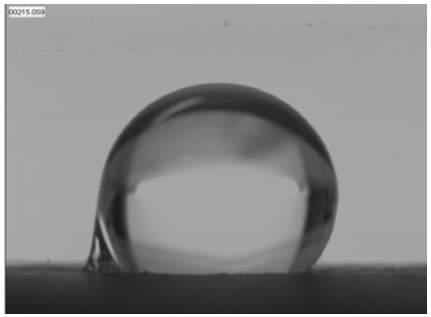

t = 90 seconds, H/2B = 0.68
θ_a = 120°, θ_r = 76°, (θ_a-θ_r) = 44°

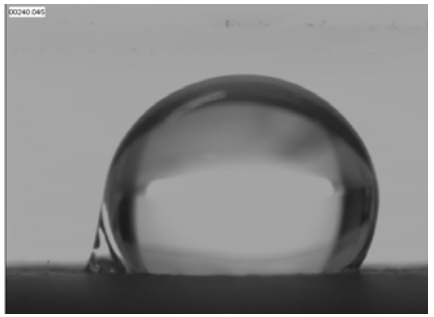

Movie clip

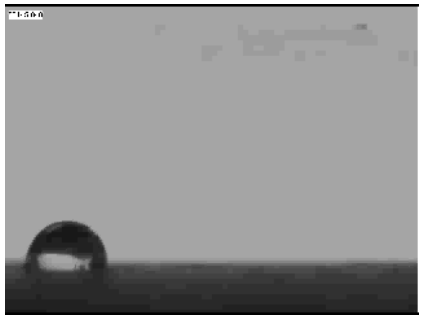

Reference: Chen, Hickner and Noble, *Int. J. Energy Research*, Vol. 29, p.1113 (2005)

Sandia National Laboratories

Analytical model for predicting instability diagrams of water-droplet removal in the low Re regime

Force balance on droplet at onset of instability:

viscous drag exerted on droplet surface = **surface tension acting on contact lines**

Schematic of droplet growing and being deformed by flowing air drag at the GDL/flow-channel interface

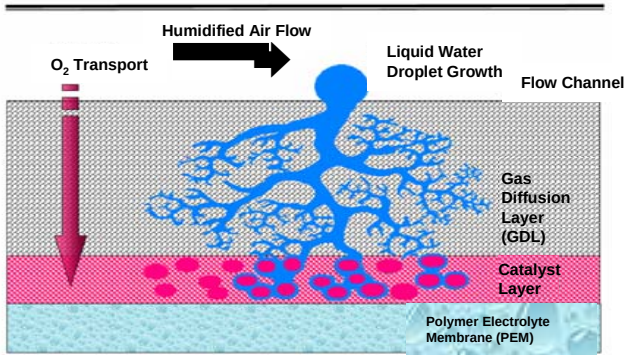

Denoting $y = \sin\frac{1}{2}(\theta_a - \theta_r)$

$\hat{H}$ – dimensionless droplet height based on channel height

$$\sin\theta_s y\sqrt{1-y^2} - \cos\theta_s y^2 - \frac{12\mu\langle v_z\rangle}{\pi\gamma\sin\theta_s}\frac{\hat{H}\left(1+\hat{H}\right)}{\left(1-\cos\theta_s\right)\left(1-\hat{H}\right)^3 + \frac{4B}{L}\hat{H}\left[1-\left(1-\hat{H}\right)^3\right]} = 0$$

A necessary condition was developed using the simplified model for preventing a fully-grown spherical water droplet from blocking the flow channel:

$$\frac{L}{B}\frac{\mu < u >}{\gamma} > \frac{\pi}{6} > \frac{\pi}{6}\sin\theta_s \sin\frac{1}{2}(\theta_a - \theta_r) > \frac{\pi}{6}\sin\theta_s \sin\frac{1}{2}(\theta_a + \theta_r)\sin\frac{1}{2}(\theta_a - \theta_r)$$

- **Rules of thumb were developed from the model: water *droplet removal* can be *enhanced* by *increasing* the channel-length-to-height *aspect ratio* and *velocity*, and *decreasing static contact angle* and its *hystetersis* ($\theta_a - \theta_r$) on GDL surface.**

Reference: Chen, Hickner and Noble, *Int. J. Energy Research*, Vol. 29, p. 1113 (2005)

Computed and measured water-droplet instability diagrams

Effect of Mean Air Flow Velocity

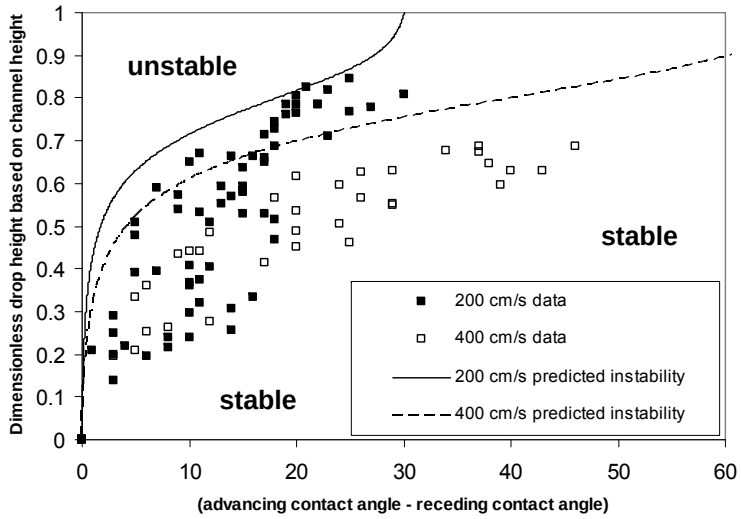

Effect of Flow Channel Length

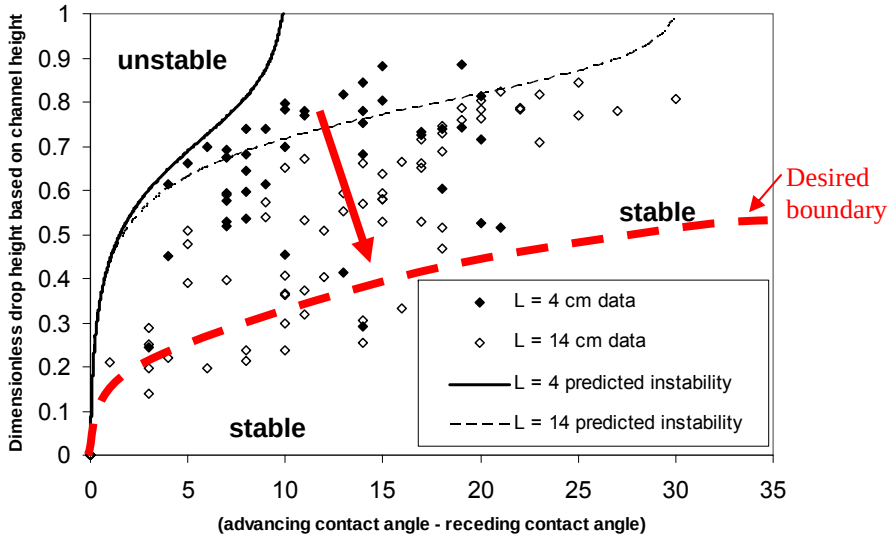

Effect of GDL Surface Treatment

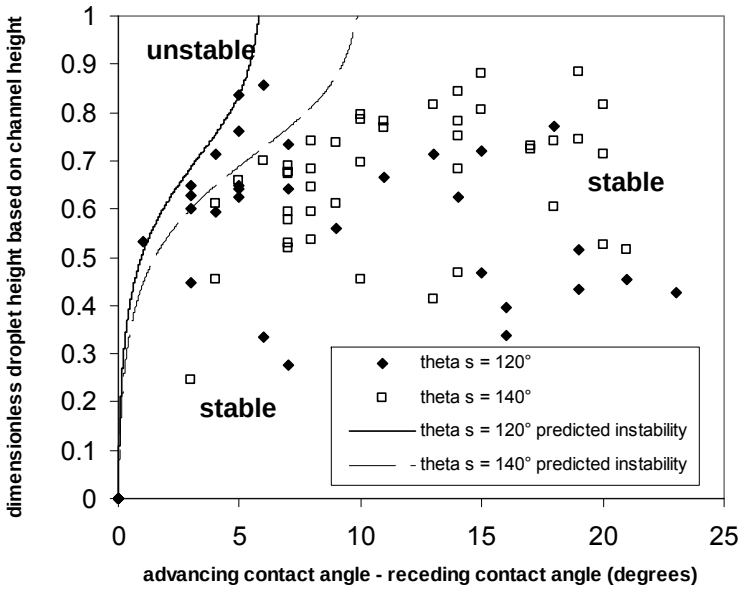

- **Simplified model yields reasonably good agreement with experimental observation.**
- **Discrepancy arises due to simplified model under-estimating drag on droplet surface.**
- **Goal: maximize unstable "window" to facilitate droplet removal.**

Reference: K. S. Chen, M. A. Hickner & D. R. Noble, *Int. J. Energy Research*, Vol. 29 (2005)

2-D finite-element simulation of laminar air flow over a cylindrical water droplet & comparison with simplified model

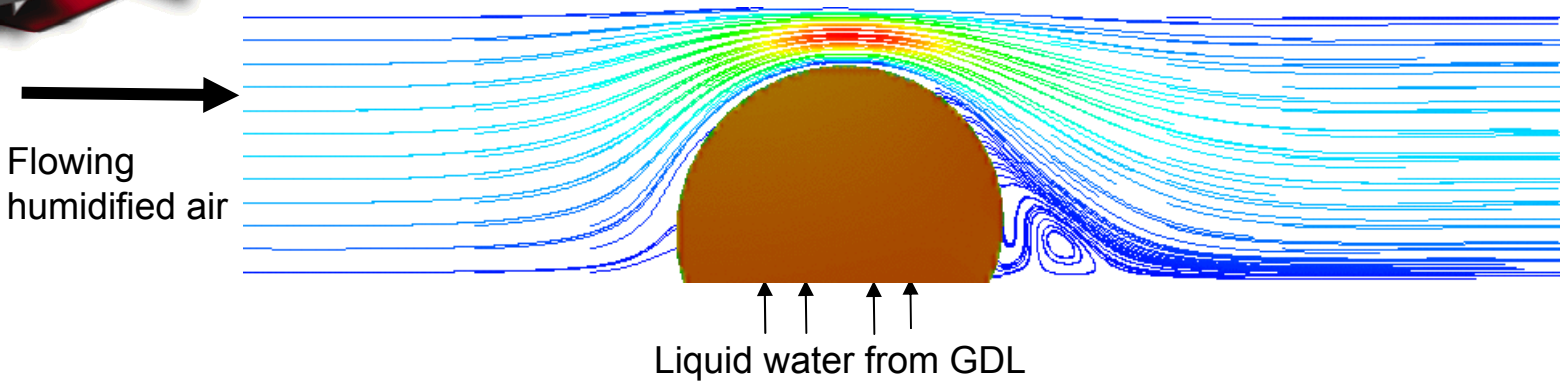

Resulting Contact Angle Hysteresis:

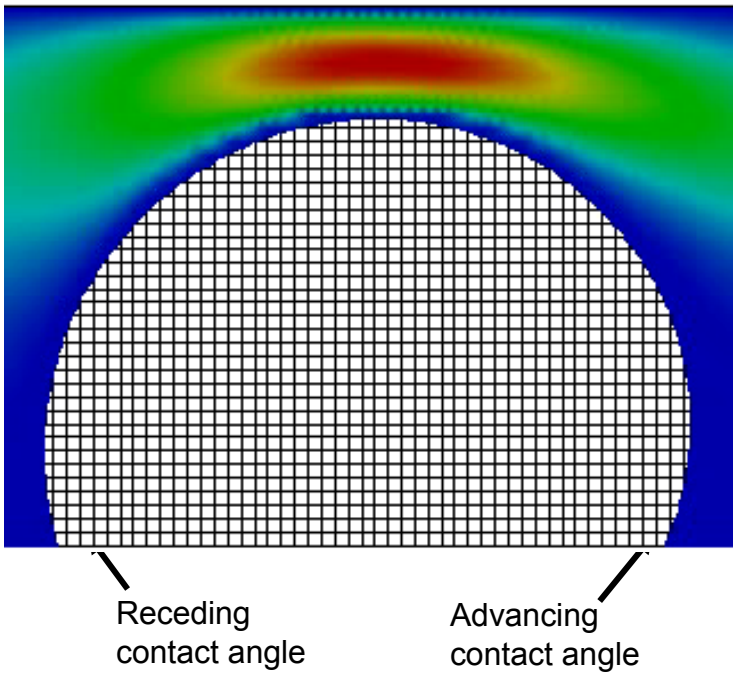

2-D FEM Simulation vs. Simplified Model Prediction

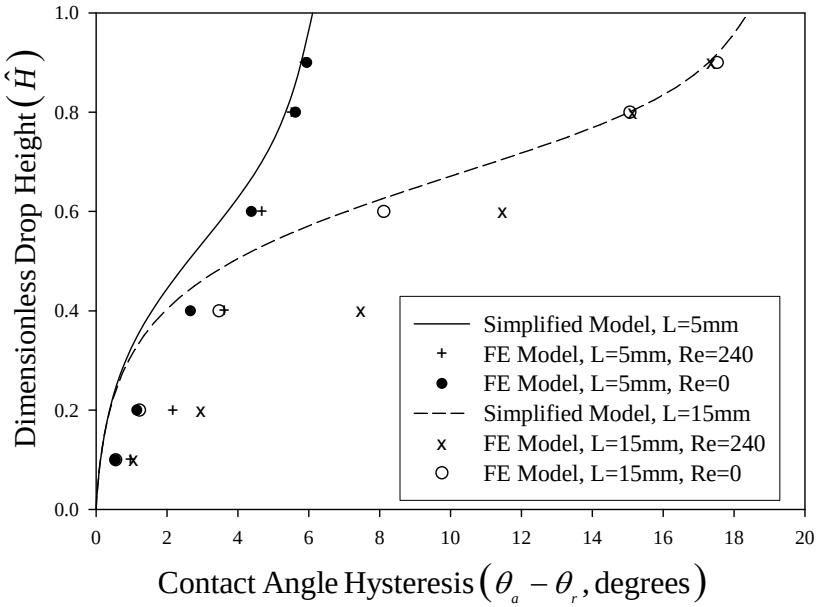

- **2-D FEM and simplified models yield reasonably good agreement for small Re.**

Reference: Chen, Hickner and Noble, *Int. J. Energy Research*, Vol. 29 (2005).

3-D numerical simulation of water-droplet detachment from the GDL/channel interface (high Re) – *Geometry*

3-D cut-away view of channel, droplet & pore

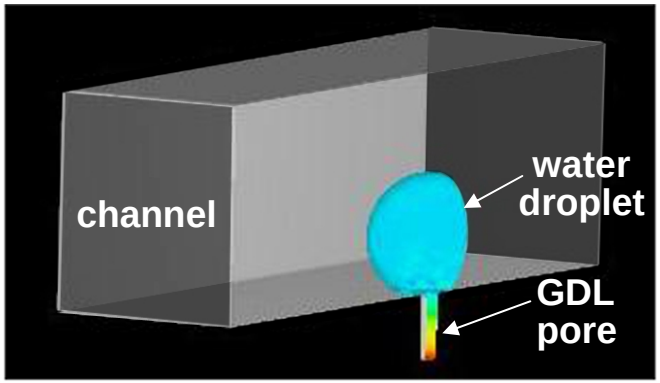

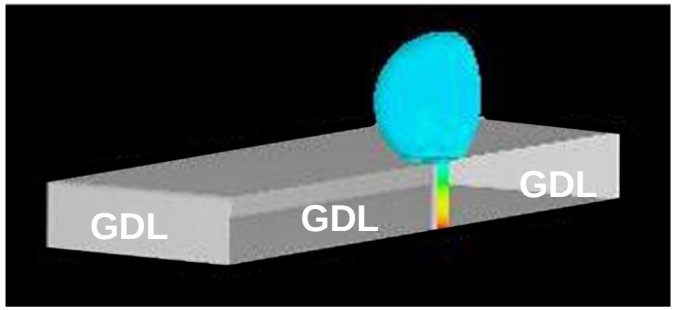

Cross-channel sectional view

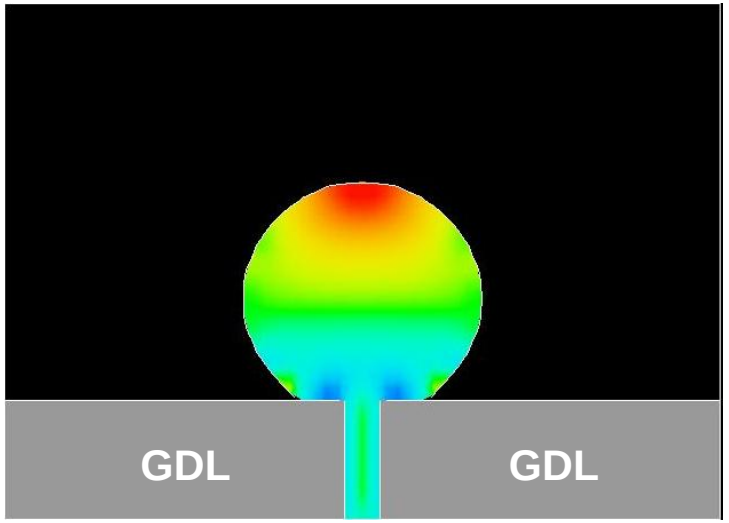

Along-channel sectional view

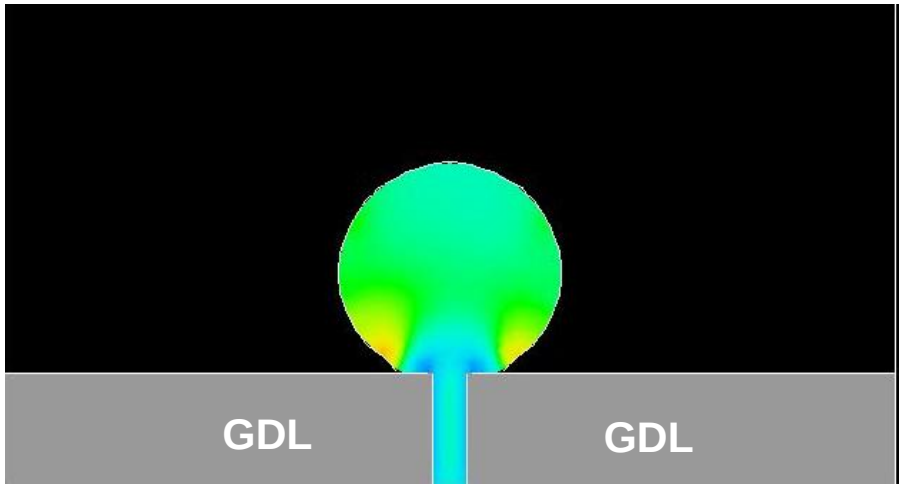

Channe/droplet/pore dimensions:

Channel height = 1 mm,
Droplet diameter = 0.6 mm,
Pore diameter = 100 μm

3-D numerical simulation of water-droplet detachment from GDL/channel interface – *Governing Equations*

Momentum conservation: $$\frac{\partial(\rho\vec{u})}{\partial t}+\nabla\cdot(\rho\vec{u}\vec{u})=-\nabla p+\nabla\cdot\left(\mu\nabla\vec{u}\right)+\rho\vec{g}+\vec{f}_{\gamma}$$

Mixture mass conservation: $$\frac{\partial\rho}{\partial t}+\nabla\cdot\rho\vec{u}=0$$

Mixture density and viscosity: $$\rho=(1-\alpha)\rho_1+\alpha\rho_2 \qquad \mu=(1-\alpha)\mu_1+\alpha\mu_2$$

Equation for liquid water fraction, α: $$\frac{\partial\left((1-\alpha)\rho_1\right)}{\partial t}+\nabla\cdot\left((1-\alpha)\rho_1\vec{u}_1\right)=0$$

or $$\frac{\partial\left(\alpha\rho_2\right)}{\partial t}+\nabla\cdot\left(\alpha\rho_2\vec{u}_2\right)=0$$

Volumetric force due to surface tension: $$\vec{f}_{\gamma}=-\gamma\kappa\cdot(\nabla\alpha)$$

Mean curvature of gas/liquid interface: $$\kappa=-\nabla\cdot\left(\frac{\nabla\alpha}{|\nabla\alpha|}\right)$$

Sandia National Laboratories

Simulated water-droplet deformation and detachment from GDL/channel interface at various air-flow velocity in the channel

1 m/s (deformation not yet visible)

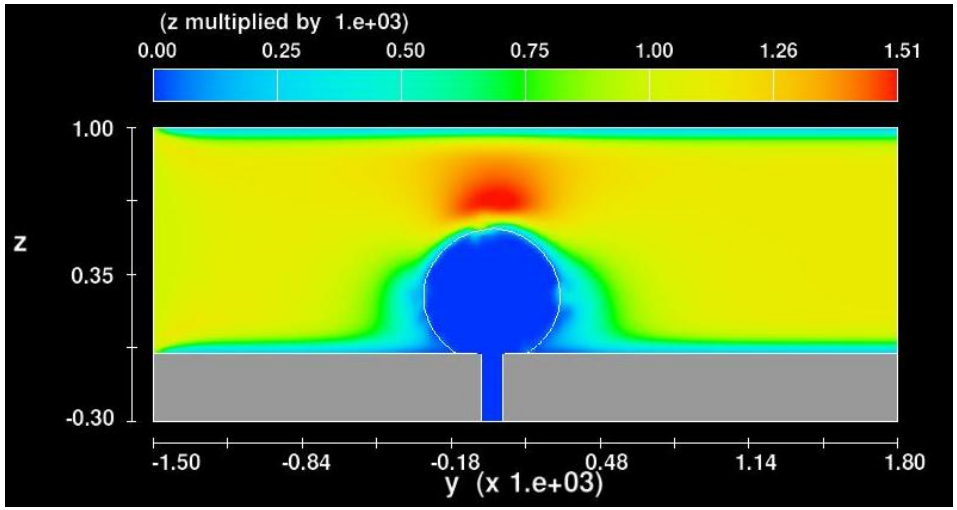

4 m/s (very visible deformation)

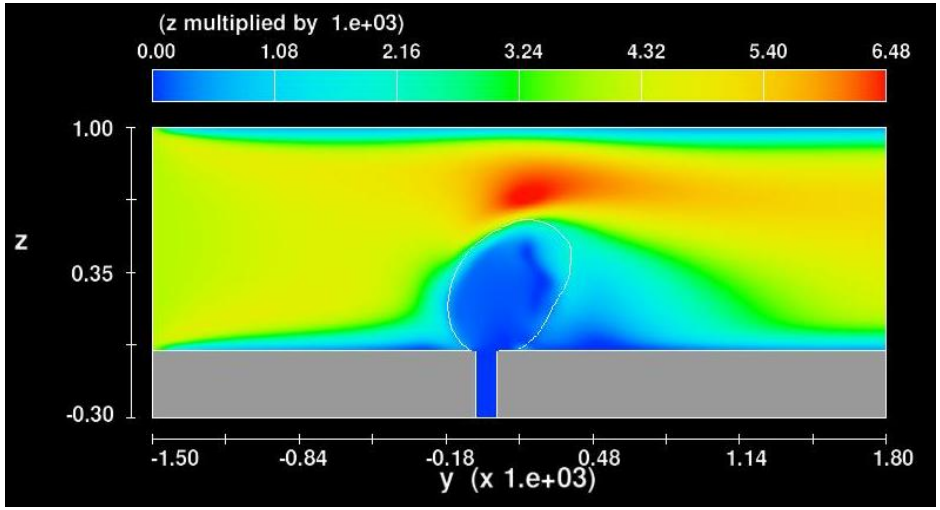

5.25 m/s (moments before detachment)

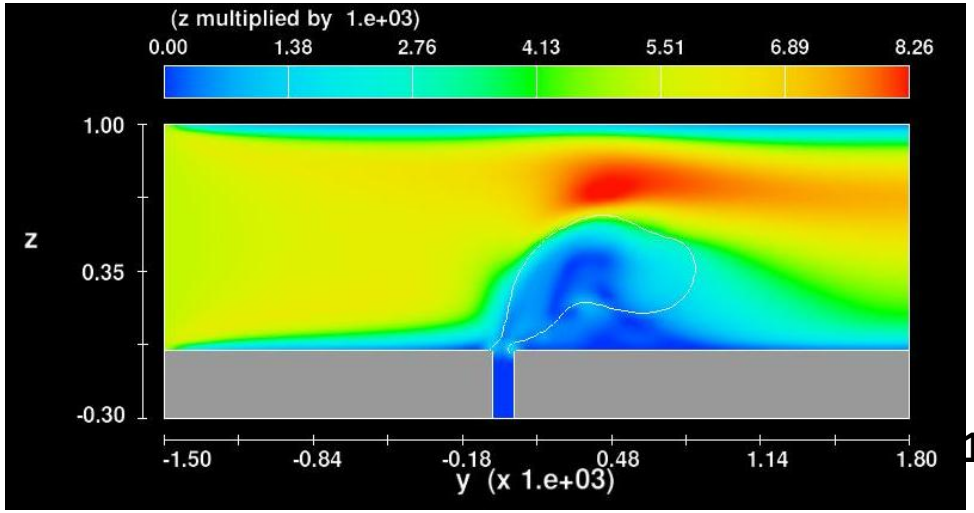

5.5 m/s (droplet was just detached)

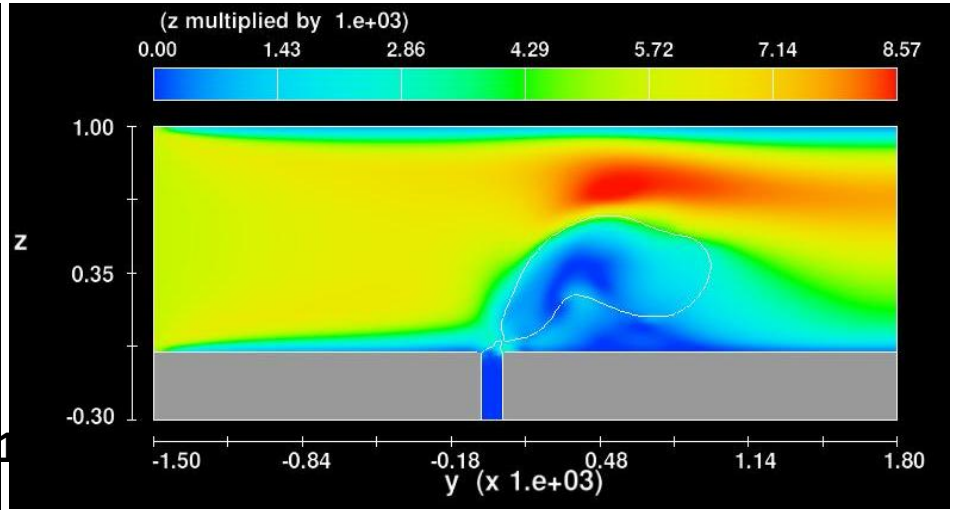

Simulated water-droplet deformation and detachment from GDL/channel interface (movie clip – static contact angle = 150°)

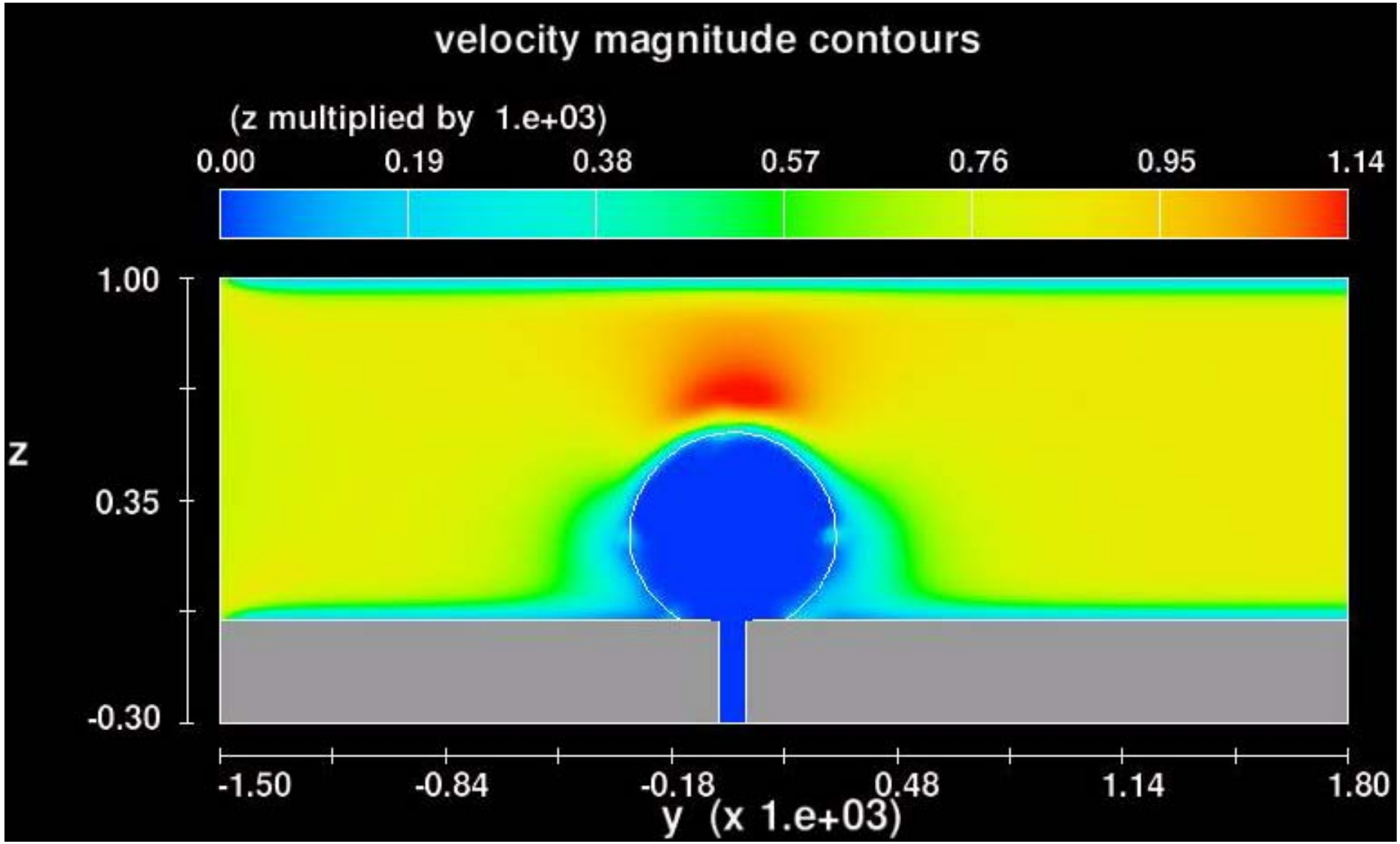

Simulated water-droplet deformation and detachment from GDL/channel interface (movie clip – static contact angle = 130°)

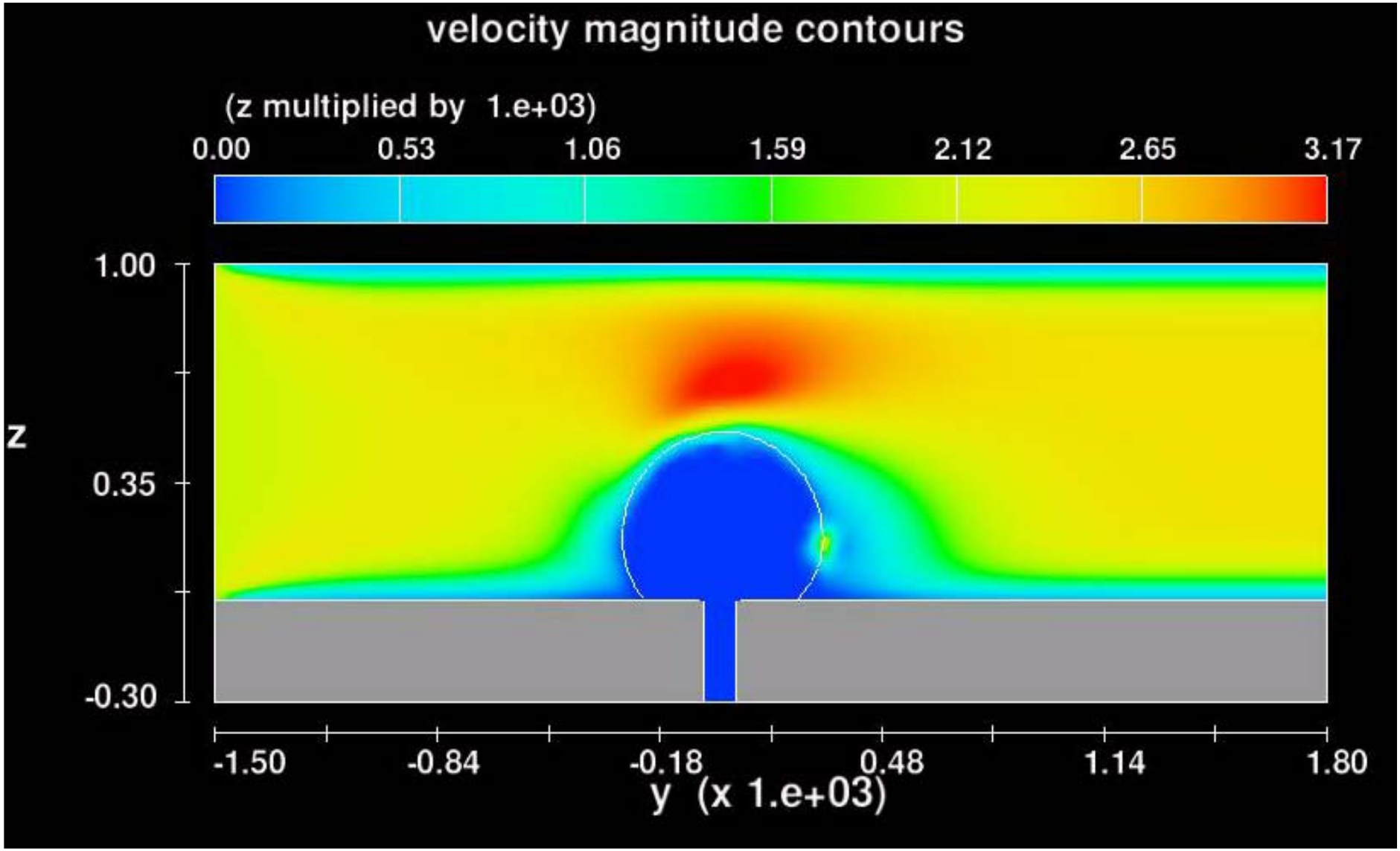

Effect of static contact angle on the onset of water-droplet detachment

Static contact angle = 150°
(carbon cloth)

Velocity at onset of droplet detachment: 5.25 m/s

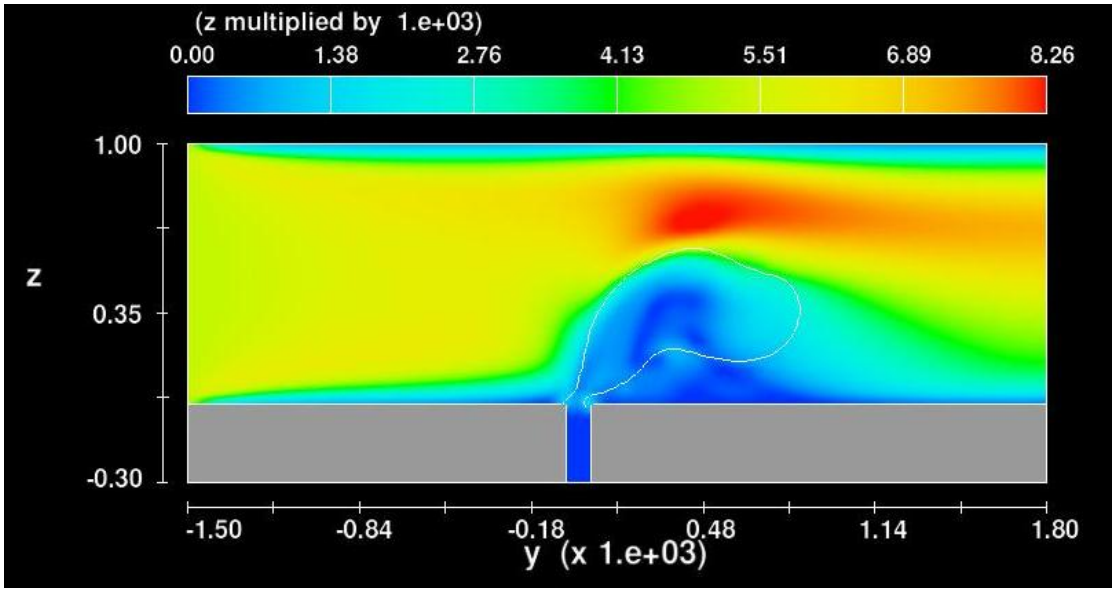

Static contact angle = 130°
(carbon paper)

Velocity at onset of droplet detachment: 6.93 m/s

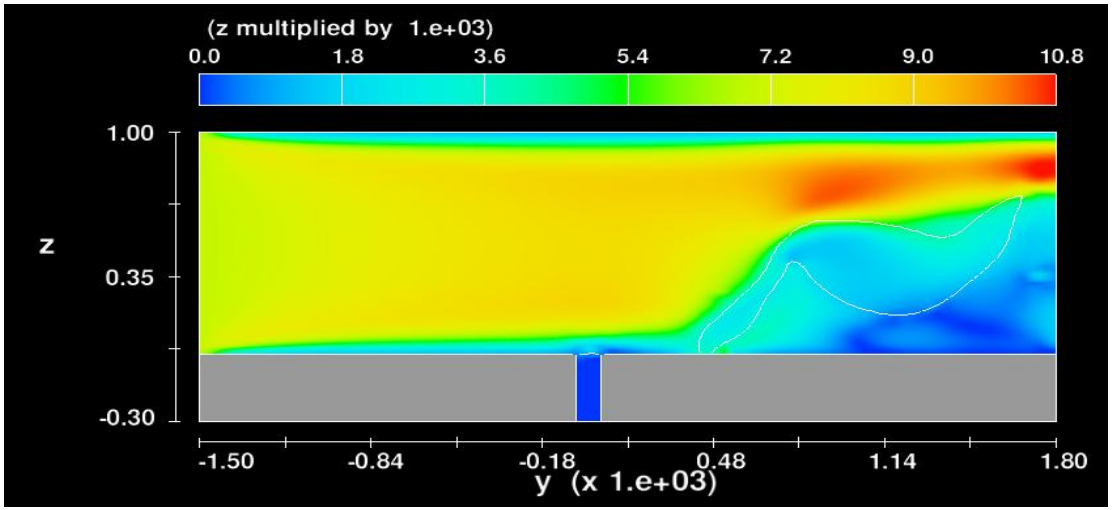

Sandia National Laboratories

- **Making GDL more hydrophobic enhances water-droplet removal!**

Simplified analytical model development (for flow regime in which pressure drag due to inertial effect dominates: 25 < Re < 2500)

Force balance on water droplet at onset of detachment:

Pressure drag exerted on droplet surface **=** **Surface tension force acting along contact lines**

$$F_d = F_\gamma$$

F_d = pressure drag exerted on the water droplet surface

F_γ = surface tension force acting along water-droplet/GDL contact lines

Sandia National Laboratories

Pressure drag exerted on droplet surface

$$F_d = A_p C_D \frac{1}{2} \rho U^2$$

Where:

A_p = projected area of droplet along flow direction

C_D = drag coefficient

ρ = density of flowing air or air-water mixture

U = average air-flow velocity in the along-channel direction.

A_p is a function of the droplet diameter and the static contact angle:

$$A_p = (\theta_s - \sin\theta_s \cos\theta_s)\frac{d^2}{4}$$

References: 1) R. Cliff, J. R. Grace, and M. E. Webber, Bubbles, Drops, and Particles, Academic Press, San Diego (1978).
2) F. M. White, Viscous Fluid Flow, McGraw-Hill, New York (1974).

Drag coefficient

For flow over a sphere in the regime in which pressure drag dominates over viscous shear, experimental data show that the drag coefficient is inversely proportional to the square root of the Reynolds number (Ref. White 1974):

$$C_D \propto \frac{1}{\sqrt{\mathrm{Re}}}$$

Taking proportionality constant to be 30 gives (this corresponds to $C_D = 1$ when $Re = 900$):

$$C_D = \frac{30}{\sqrt{\mathrm{Re}}} \quad \text{where} \quad \mathrm{Re} = \frac{\rho U H_c}{\mu}$$

with H_c being the channel height

Reference: F. M. White, Viscous Fluid Flow, p. 203 – 210, McGraw-Hill, New York (1974).

Surface tension force tending to hold water droplet in place

$$F_\gamma = \pi \frac{d}{2} \gamma \sin\theta_s (\cos\theta_r - \cos\theta_a)$$

Simplifying using trigonometry relations:

$$F_\gamma = \pi d \gamma \sin^2 \theta_s \sin \frac{1}{2}(\theta_a - \theta_r)$$

where θ_s = static contact angle, θ_a = advancing contact angle, θ_r = receding contact angle, $\theta_a - \theta_r$ = contact-angle hysteresis.

- Surface tension force decreases with increasing static contact angle and reducing contact-angle hysteresis.

Simplified analytical model

$$V_c = \left[\frac{H_c}{\rho\mu}\right]^{1/3}\left[\frac{\pi\gamma\sin^2\theta_s\sin\frac{1}{2}(\theta_a-\theta_r)}{5(\theta_s-\sin\theta_s\cos\theta_s)d}\right]^{2/3}$$

Where: d = water droplet diameter, H_c = channel height, ρ = density, μ = viscosity, γ = surface tension, θ_s = static contact angle, θ_a = advancing contact angle, θ_r = receding contact angle, $\theta_a - \theta_r$ = contact-angle hysteresis.

- **The critical air-flow velocity increases rapidly with decreasing droplet size ($V_c \sim d^{-2/3}$); V_c also increases with raising channel height and decreasing ρμ.**
- **Making GDL surface more hydrophobic (i.e., increasing static contact angle, θ_s) and less rough (i.e., lowering contact-angle hysteresis) reduces critical velocity, V_c.**

Model validation – comparison with experimental data of Zhang et al.* and Theodorakakos et al.**

Data by Zhang et al. (2006)*

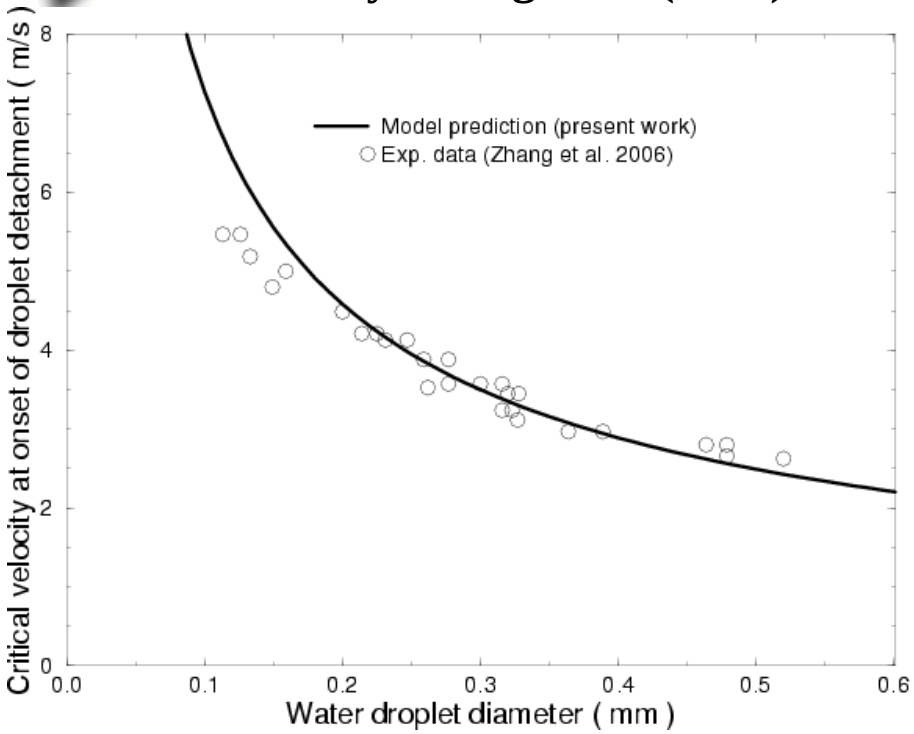

Data by Theodorakakos et al. (2006)**

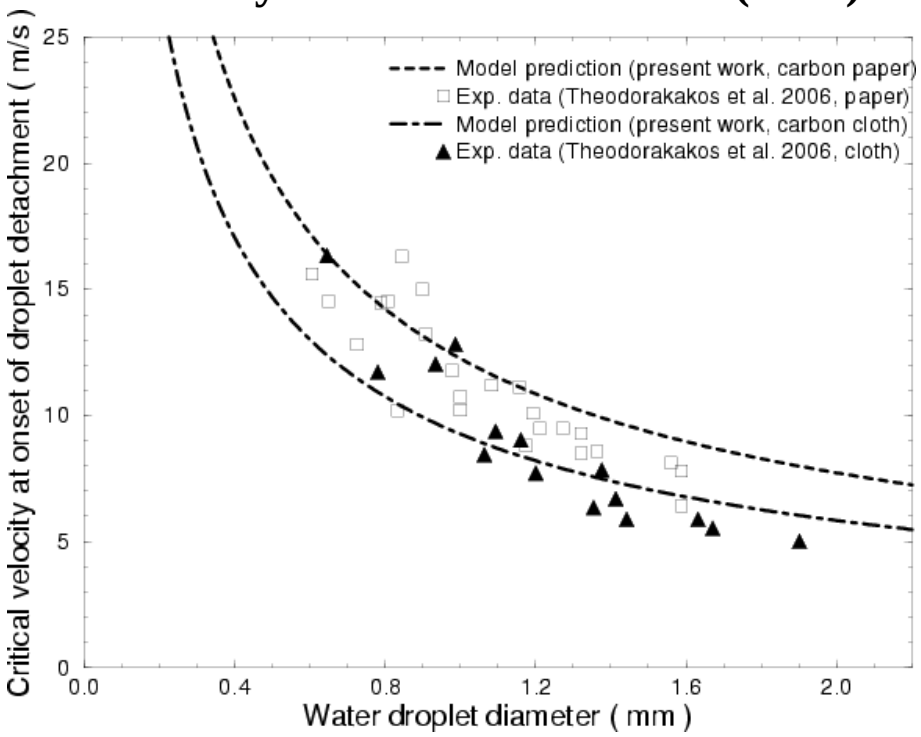

- **Agreements between model predictions and experimental data are reasonably good!**

* **F. Y. Zhang, X. G. Yang, and C. Y. Wang, *J. Electrochem. Soc.*, 153 (2) A225–A232 (2006).**

** **A. Theodorakakos, T. Ous, M. Gavaises, J. M. Nouri, N. Nikolopoulos, and H. Yanagilhara, *J. Colloid Interface Sci.*, 300, p. 673–687 (2006).**

Parameters used in model validation case studies

	Channel height (H_c, mm)	Static contact angle (θ_s, degrees)	Contact-angle hysteresis ($\theta_a - \theta_r$, degrees)
Zhang et al.* (carbon paper GDL)	**0.5**	**150**	**10**
Theodorakakos et al. (carbon paper GDL)**	**2.7**	**130**	**35**
Theodorakakos et al. (carbon cloth GDL)**	**2.7**	**145**	**45**

* F. Y. Zhang, X. G. Yang, and C. Y. Wang, "Liquid water removal from a polymer electrolyte fuel cell", *J. Electrochem. Soc.*, **153** (2) A225–A232 (2006).

** A. Theodorakakos, T. Ous, M. Gavaises, J. M. Nouri, N. Nikolopoulos, and H. Yanagilhara, "Dynamics of water droplets detached from porous surfaces of relevance to PEM fuel cells", *J. Colloid Interface Sci.*, **300**, p. 673–687 (2006).

Effects of static contact angle and contact-angle hysteresis on critical air-flow velocity

Effect of static contact angle

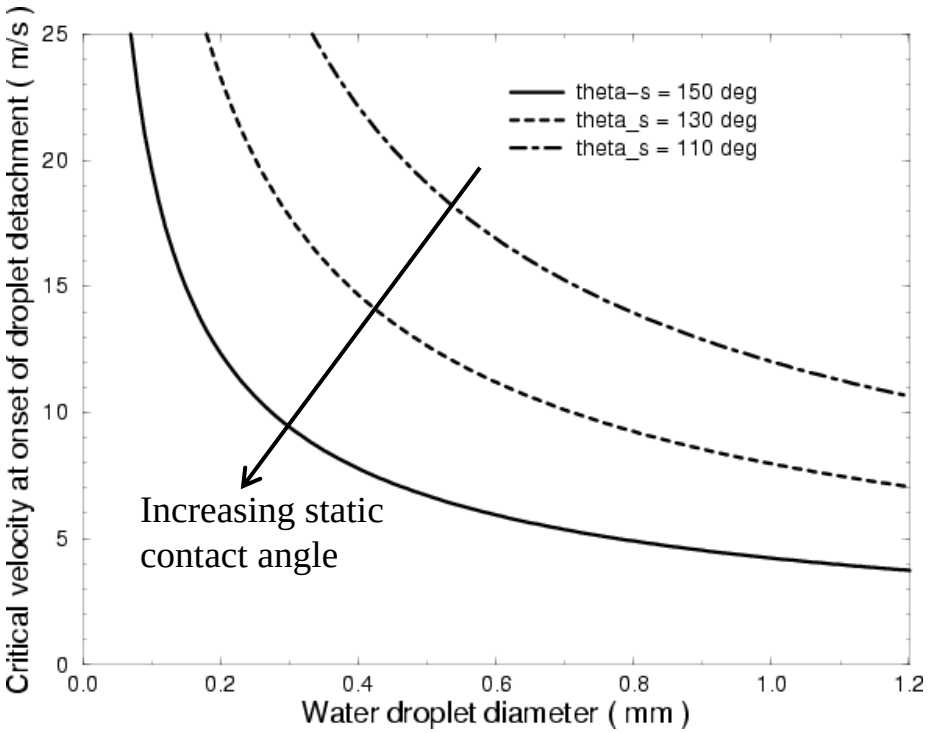

Effect of contact-angle hysteresis

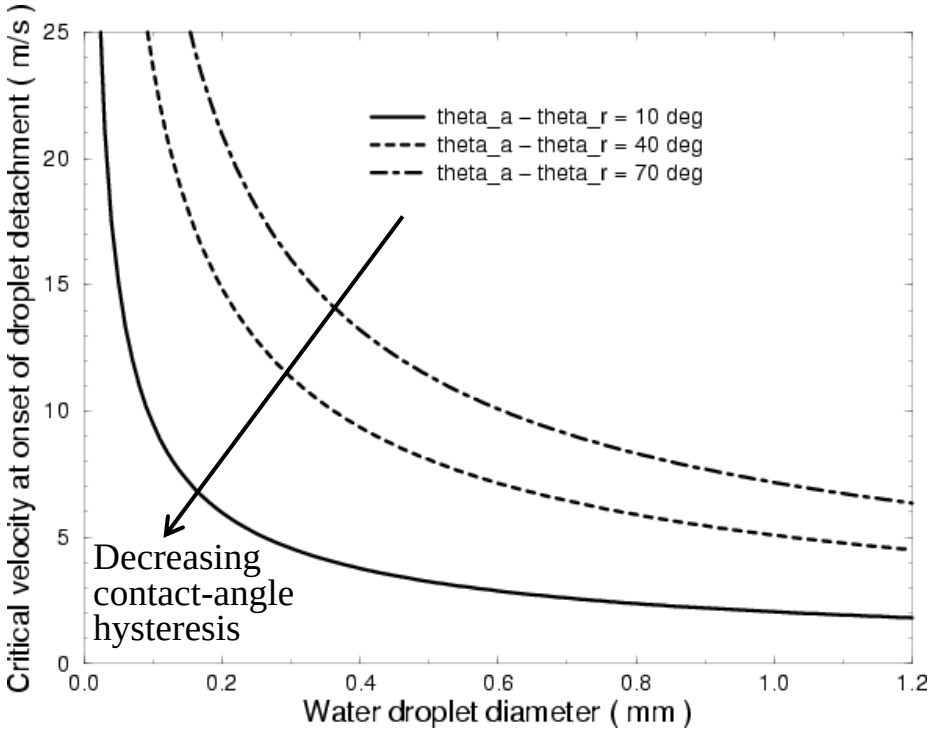

- **Making GDL more hydrophobic reduces the critical velocity required to detach water droplets.**
- **Decreasing contact-angle hysteresis (e.g., reducing GDL surface roughness) enhances droplet removal.**

Sandia National Laboratories

Effects of channel height and ρμ product on critical air-flow velocity

Effect of channel height

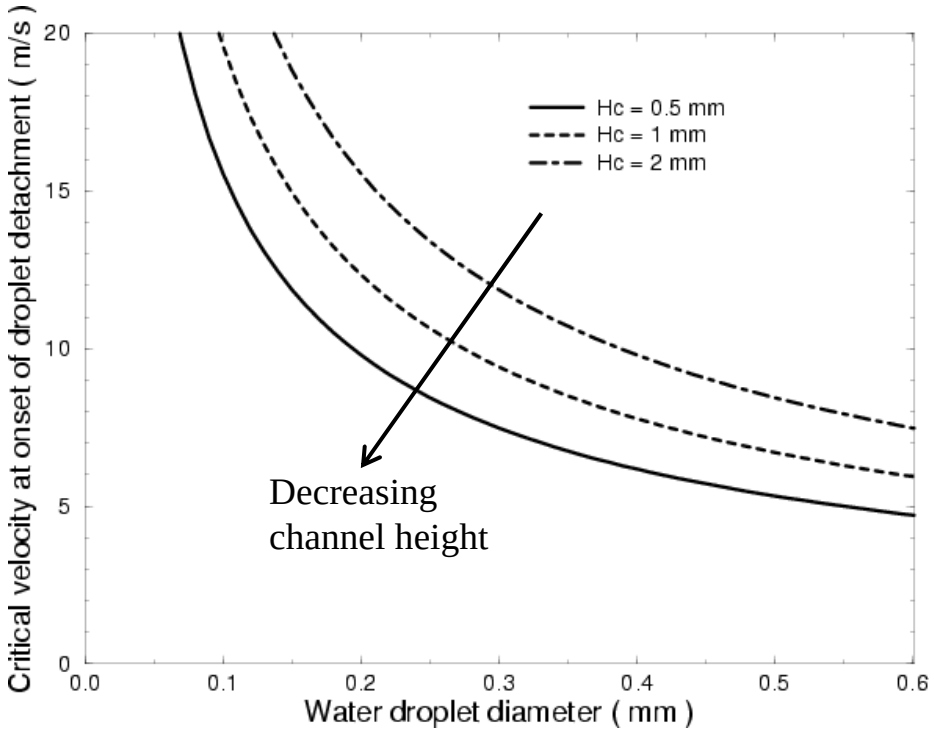

Effect of ρμ product
(in terms of liquid water saturation in flowing mixture)

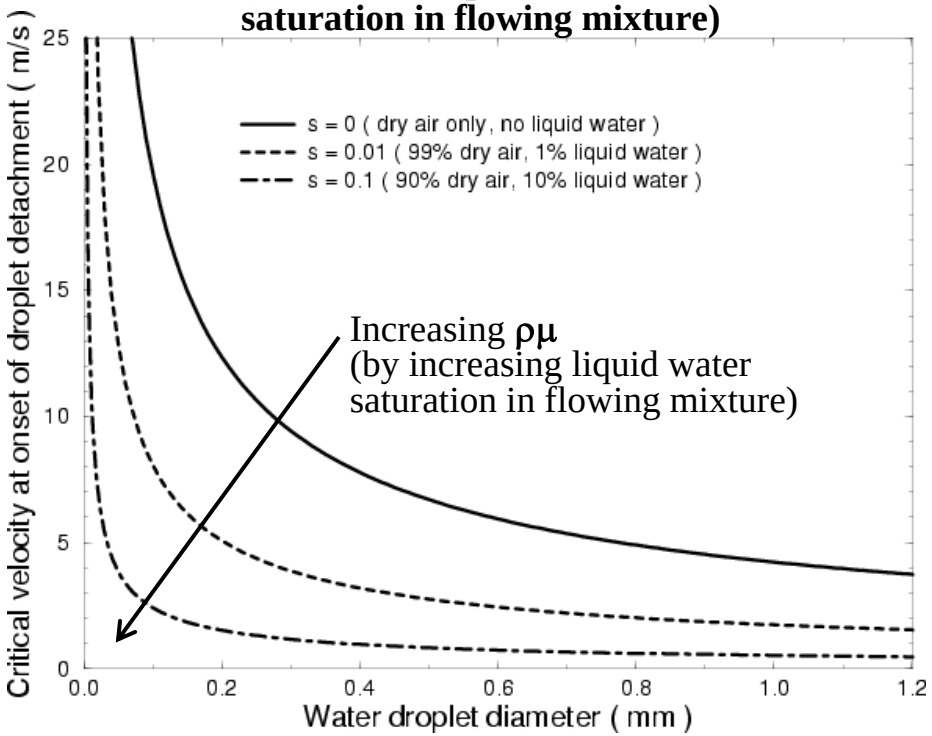

- **Decreasing channel height reduces the critical velocity required to detach water droplets.**
- **Increasing ρμ (by increasing liquid water saturation in the flowing air/liquid-water mixture) enhances droplet removal.**

Sandia National Laboratories

Effect of microporous layer on water transport across PEMFC membrane

- **Micro-porous sub-layer**
  - **Micro-particles**
    - » PTFE (i.e. Teflon) and C
  - **Smaller pore size**
    - » (200-1000 nm)
- **Advantages:**
  - **Improve water management**
    - » Reduced catalyst layer flooding
    - » Increased water flux towards anode
  - **Better electronic contact between catalyst layer and GDL**

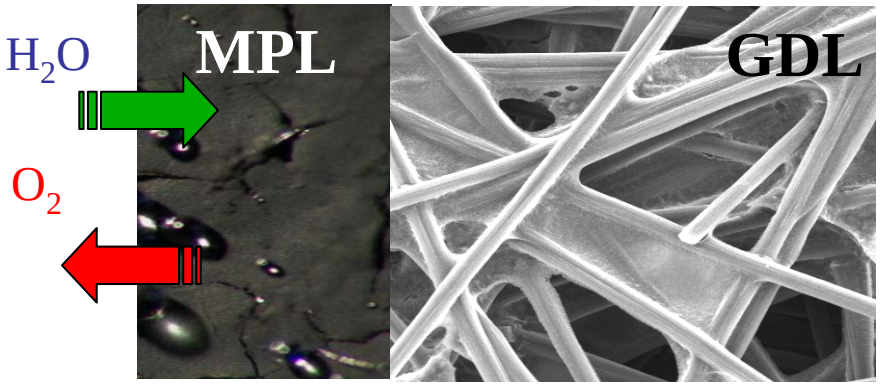

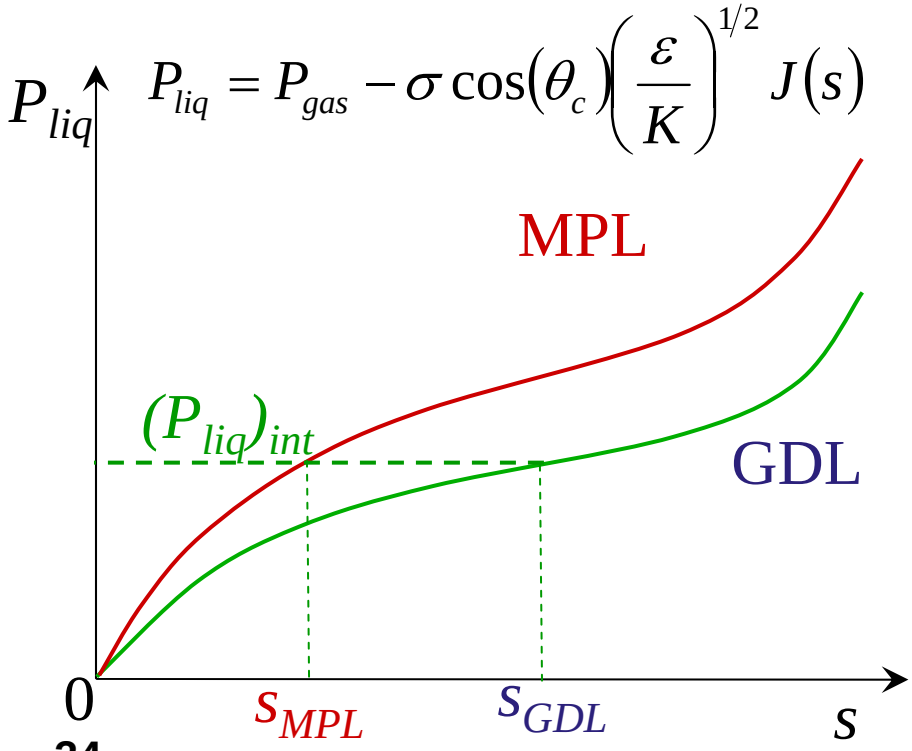

Sandia National Laboratories

Reference: U. Pasaogullari, C.Y. Wang, K.S. Chen, *J. Electrochem. Soc., 152, A1574 (*2005).

Equations governing transport in a simplified cell having a cathode MPL

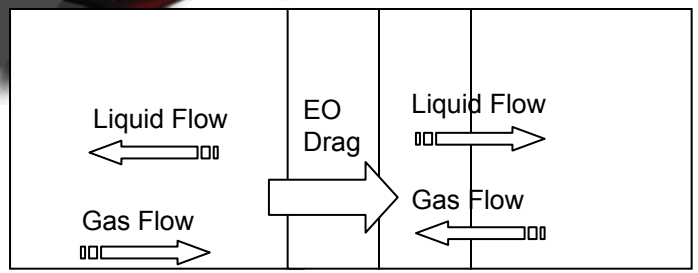

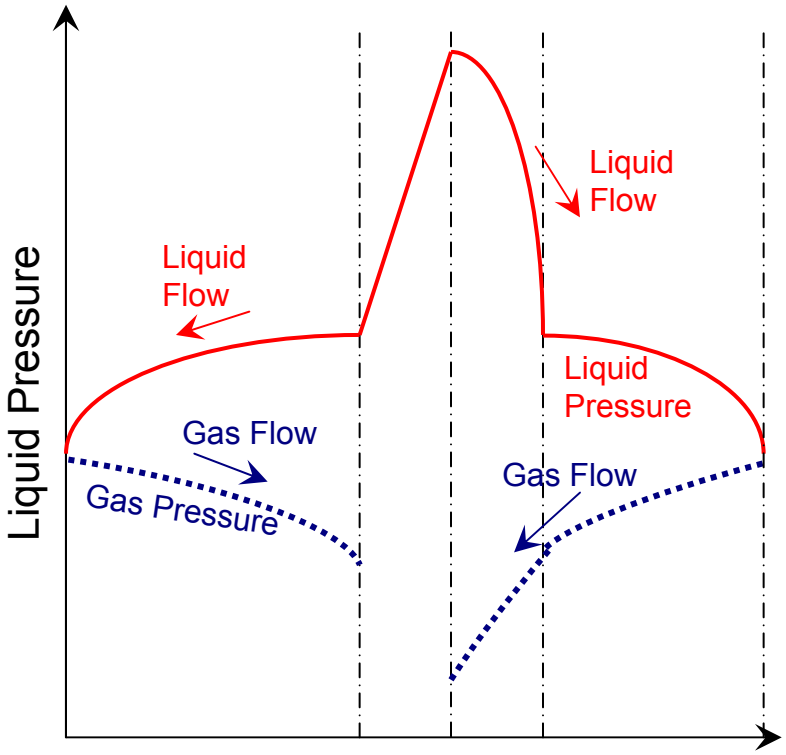

- **M^2 Formulation (Wang & Cheng, 1997)**
  - **Continuity**

$$\frac{\partial(\rho\varepsilon)}{\partial t}+\nabla\cdot(\rho\vec{u})=0 \qquad \rho=\rho_l\cdot s+\rho_g\cdot(1-s)$$

  - **Momentum (Darcy's law)**

$$\nabla p_k=-\frac{\mu_k}{Kk_{rk}}\vec{u}_k$$

  - **Species Conservation**

$$\varepsilon\frac{\partial(C^i)}{\partial t}+\nabla\cdot(\gamma_c\vec{u}C^i)=\nabla\cdot\left[\varepsilon D_g^{i,eff}(1-s)\nabla C_g^i\right]-\nabla\cdot\left[\left(\frac{\mathrm{mf}_l^i}{M^i}-\frac{C_g^i}{\rho_g}\right)\vec{j}_l\right]$$

$$\gamma_c=\begin{cases}\dfrac{\rho}{C^{H2O}}\left(\dfrac{\lambda_l}{M^{H2O}}+\dfrac{\lambda_g}{\rho_g}C_{sat}\right) & \text{for water}\\[2ex] \dfrac{\rho\lambda_g}{\rho_g(1-s)} & \text{for other species}\end{cases}$$

$$\vec{j}_l=\frac{\lambda_l\lambda_g}{\nu}K\nabla P_c \quad \text{where} \quad P_c=\sigma\cos(\theta_c)\left(\frac{\varepsilon}{K}\right)^{1/2}J(s)$$

$$s=\frac{C^{H_2O}-C_{sat}^{H_2O}}{\rho_l/M^{H_2O}-C_{sat}^{H_2O}} \qquad \lambda_l=\frac{k_{rl}/\nu_l}{k_{rl}/\nu_l+k_{rg}/\nu_g} \qquad \lambda_g=1-\lambda_l$$

Sandia National Laboratories

Sample model prediction: computed effect of microporous layer on net water transport across membrane

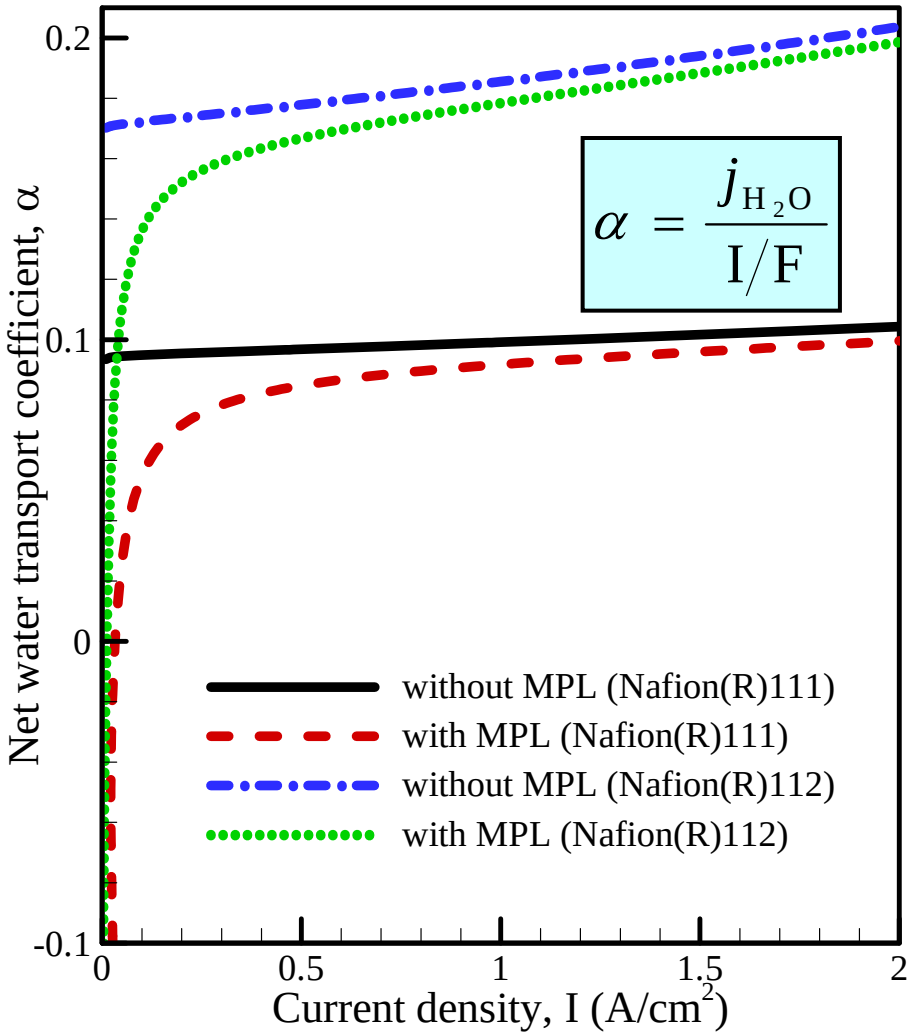

- **● MPL significantly improves the back flux of water towards anode**
  - **– Reduced Flooding**
  - **– Improving the hydration of membrane on the anode side**
- **● Decreasing pore size and porosity and increasing contact angle and thickness of MPL**

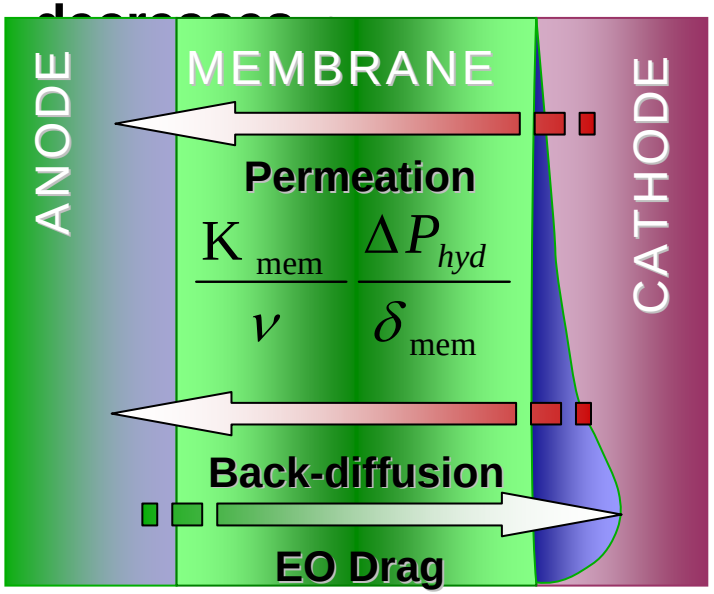

Sandia National Laboratories

Reference: U. Pasaogullari, C.Y. Wang, K.S. Chen, *J. Electrochem. Soc., 152, A1574 (*2005).

Sample model prediction: computed effects of MPL properties on net water transport across membrane

Effect of contact angle (hydrophobicity) in micro-porous layer on net water transport

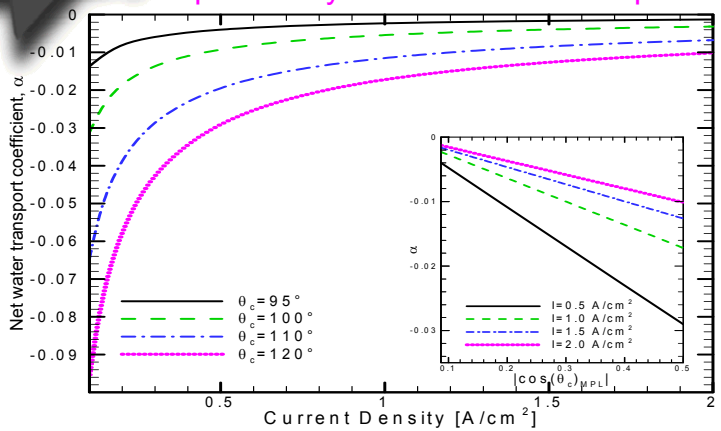

Effect of mean pore size in micro-porous layer on net water transport

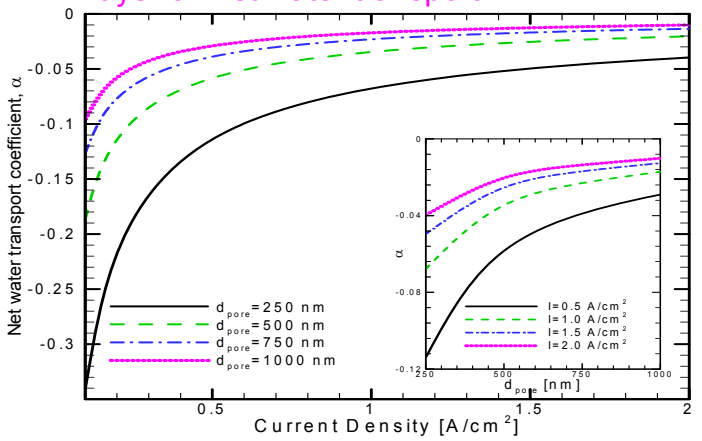

Effect of thickness in micro-porous layer on net water transport

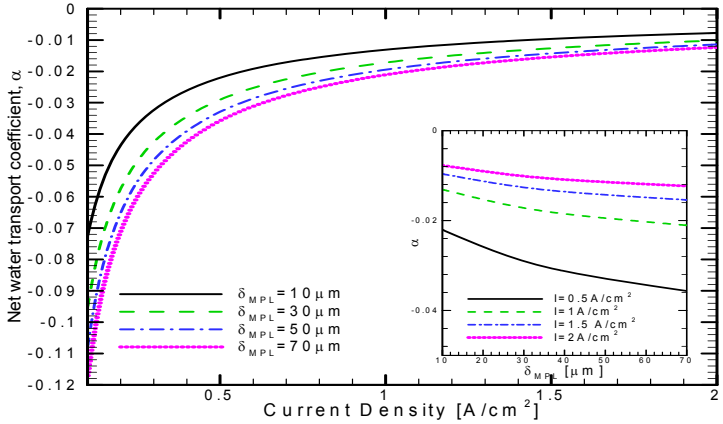

Effect of mean porosity in micro-porous layer on net water transport

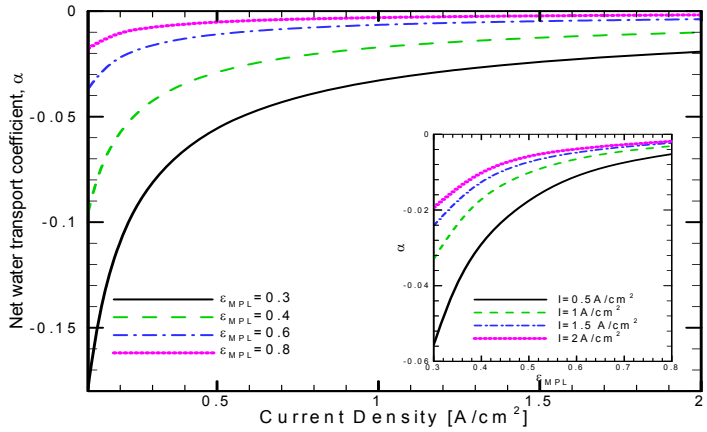

- **Net water transport to and thus flooding in the cathode can be reduced by**

1) making the micro-porous layer more hydrophobic; 2) increasing micro-porous layer thickness; 3) decreasing micro-porous layer mean pore size; and 4) decreasing mean porosity.

Sandia National Laboratories

Reference: U. Pasaogullari, C.Y. Wang, K.S. Chen, *J. Electrochem. Soc., 152, A1574 (*2005).

Modeling two-phase flow mal-distribution among PEM fuel-cell channels

Two Phase Phenomena in PEMFC Flow Channels

- Product water transports into the cathode channels from the cathode GDL (We assume it to be uniform)
- As the gas flow moves downstream, the water vapor concentration increases till saturation, and then liquid water forms in the channel.
- Once two-phase flow forms in a channel, the flow resistance increases, thereby reducing the flow rate in that channel under constant pressure drop.
- Low flowrate further promotes liquid water accumulation, causing flow mal-distribution in multiple, parallel channels and eventually clogging the flow channel(s).
- At very low flow rate, liquid water could not be flushed out due to capillary wicking in hydrophilic corners.

Reference: S. Basu, Y. Wang, C. Y. Wang and K. S. Chen, "Two-phase flow maldistribution and mitigation in polymer electrolyte fuel cells", to appear in *J. Fuel Cell Science and Technology* (in press).

Operating at high current density and high stoichiometric flow ratio can help flush liquid water from a few channels – a case study with seven channels

Saturation contours

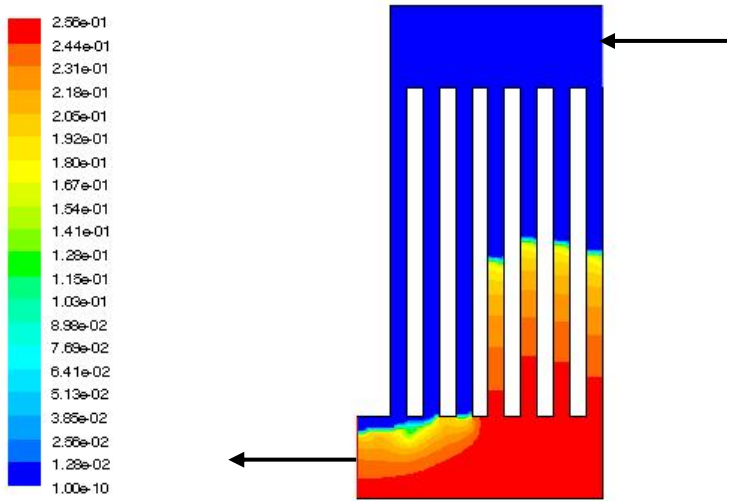

Velocity contours

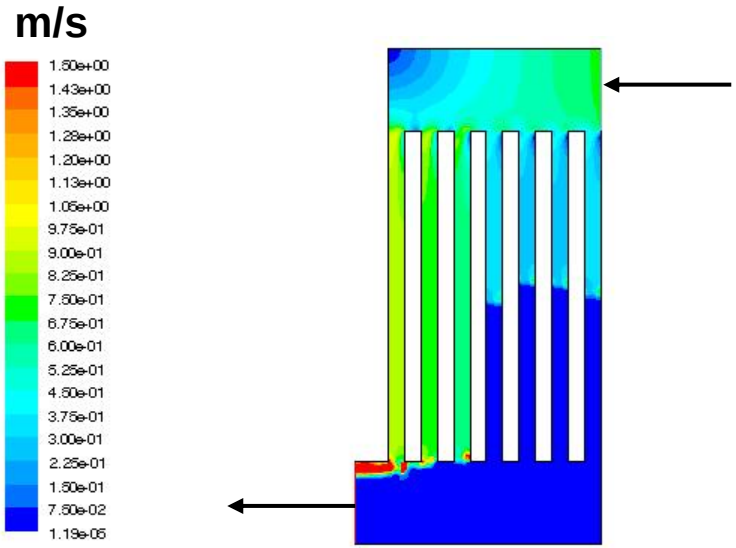

Operating conditions:

i = 0.8A/cm^2 and stochiometric flow ratio = 4

Sandia National Laboratories

Elucidating rate of phase change (condensation/evaporatio) in PEM fuel cells – motivation

- To find out where phase changes take place within the cell
- To help determine the desired range of operating parameters such as cell temperature, relative humidity, stoic, etc.

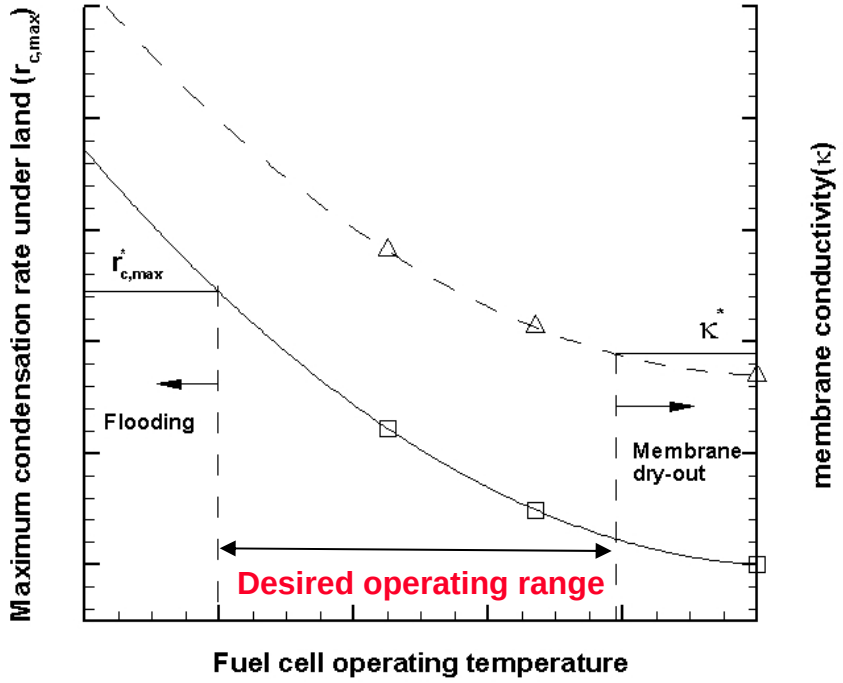

Sandia National Laboratories

Governing equations for computing *phase-change rate* in PEM fuel cells using the M² (multiphase mixture) model

- **Mass:** $$\nabla \cdot (\rho \vec{u}) = 0$$
- **Momentum:** $$\frac{1}{\varepsilon^2} \nabla \cdot (\rho \vec{u} \vec{u}) = -\nabla P - \nabla \cdot (\rho \tau) + \frac{\nu}{K} (\rho \vec{u})$$
- **Energy:** $$\nabla \cdot (\gamma_T \rho C_p \vec{u} T) = \nabla \cdot (k_{eff} \nabla T) + S_T$$
- **Species:** $$\nabla \cdot (\gamma_c \vec{u} C^k) = \nabla \cdot (D_g^{k,eff} \nabla C_g^k) - \nabla \cdot [(\frac{m f_l^k}{M^k} - \frac{C_g^k}{\rho_g}) \vec{j}_l] + S_c$$
- **Charge (Electrons):** $$0 = \nabla \cdot (\sigma^{eff} \nabla \Phi_s) + S_{\Phi_s}$$
- **Charge (Protons):** $$0 = \nabla \cdot (k^{eff} \nabla \Phi_e) + S_{\Phi_e}$$

References: 1) C.-Y. Wang and P. Cheng, *Inter. J. Heat & Mass Transfer,* Vol. 39, pp. 3607 (1996).
2) H. Ju, G. Luo, and C.-Y. Wang, *J. Electrochem. Soc.*, Vol. 154, pp. B218-B228 (2007).
3) S. Basu, C.-Y. Wang, K. S. Chen, manuscript draft for *6th ASME Fuel Cell Conference*.

Computing rate of phase change (condensation/evaporation) in PEM fuel cells

- **Define phase-change rate as follows:**

$$r_{H2O} = H(C_{H2O} - C_{sat})$$

- **In GDL mass transfer coefficient H is on the order of 10^5 s^{-1}.**
- **Interfacial equilibrium is reached when H > 5000.**
- **Hence, saturation or liquid-water volume fraction is defined by assuming interfacial equilibrium between the phases:**

$$s = \frac{C^{H_2O} - C_{sat}^{H_2O}(T)}{\rho_l / M_{H_2O} - C_{sat}^{H_2O}(T)}$$

References: 1) C.Y. Wang, W. B. Gu and J. Liaw, *J. Electrochem. Soc.*, Vol.145, pp. 3407, (1998).
2) H. Meng, *Journal of Power Sources*, Vol. 168-1, pp. 218, (2007).

Computing Phase-Change Rate
(Continued)

- **Phase-change rate can be computed from the mass conservation equation in the liquid phase.**

$$\dot{m} = \nabla \cdot (\rho_l u_l)$$

- **The liquid flux is defined in terms of capillary flux and mixture flux as (cf. Wang and Cheng, 1996):**

$$\rho_l u_l = j_l(s) + \lambda_l(s)\rho u$$

Reference: C.Y. Wang and P. Cheng, *Inter. J. Heat & Mass Transfer,* Vol. 39, pp. 3607 (1996).

Model geometry and cross sections for analysis

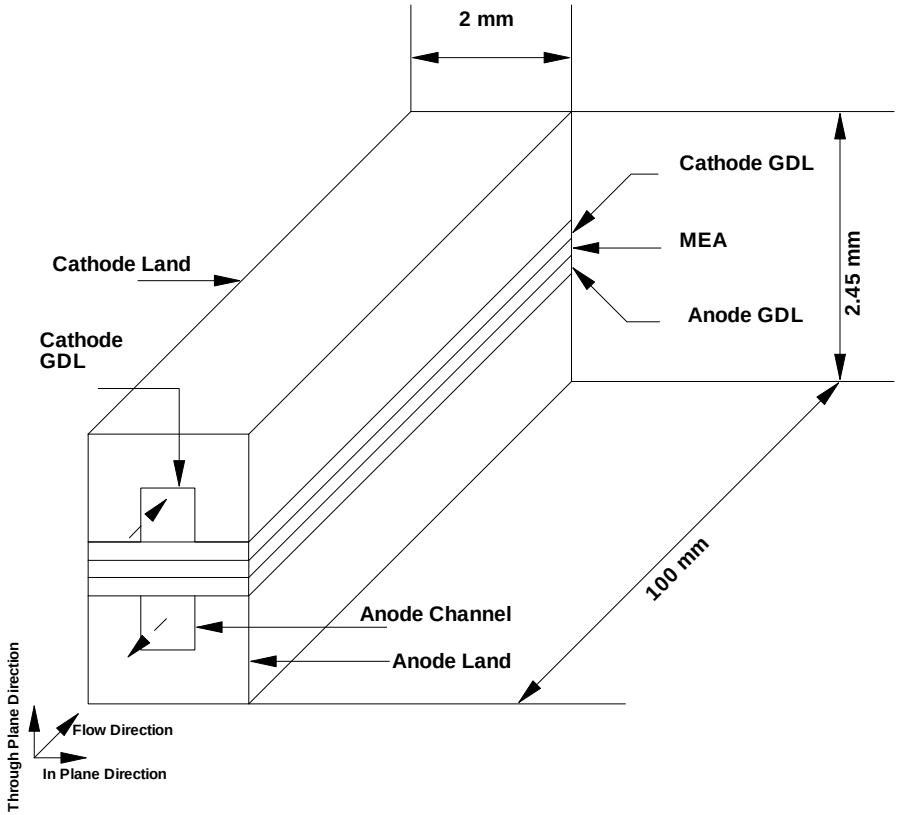

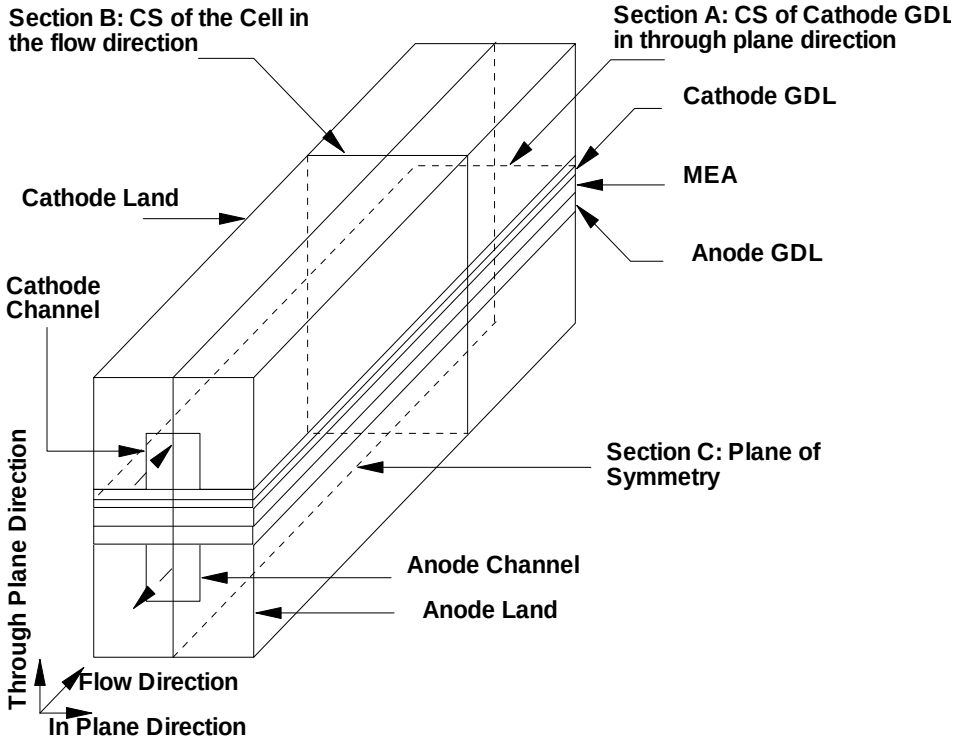

Sandia National Laboratories

Effect of Inlet Humidity on Temperature (I=1.0A/cm2, St=2.0, at Section B)

100% RH

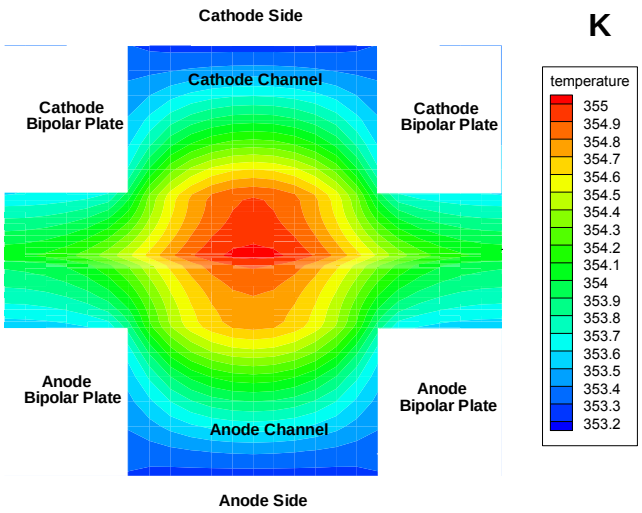

67% RH

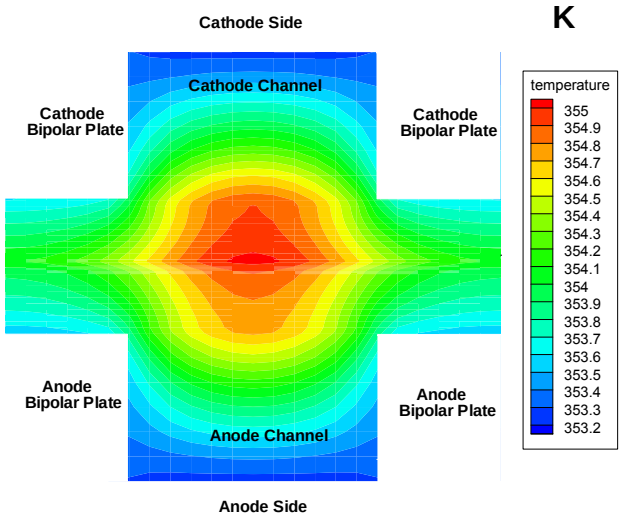

45% RH

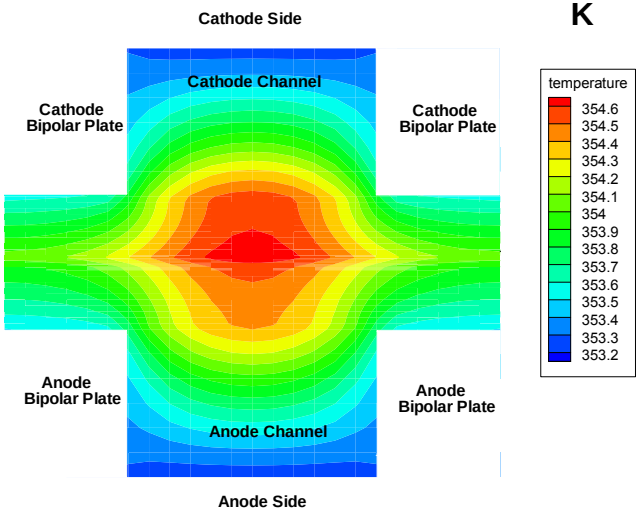

- **Section is taken at midway between the inlet and exit at section B.**
- **Temperature is high in the channel but low under the land due to higher conductivity of bipolar plate.**
- **Temperature rises less rapidly as inlet humidity is decreased.**

Sandia National Laboratories

Effect of Inlet Humidity on Liquid Saturation (I=1.0A/cm2, St=2.0, at Section B)

100% RH

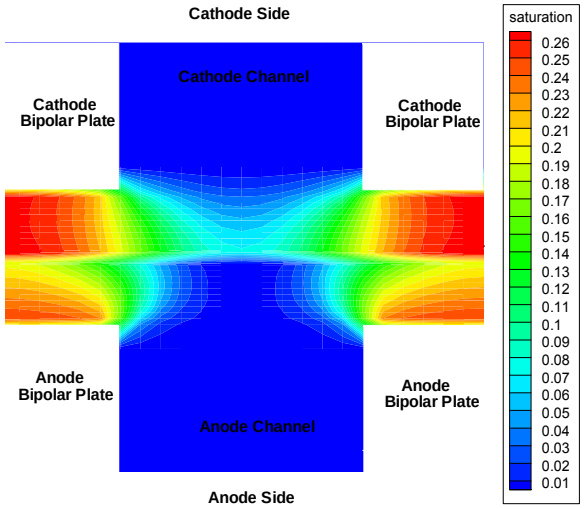

67% RH

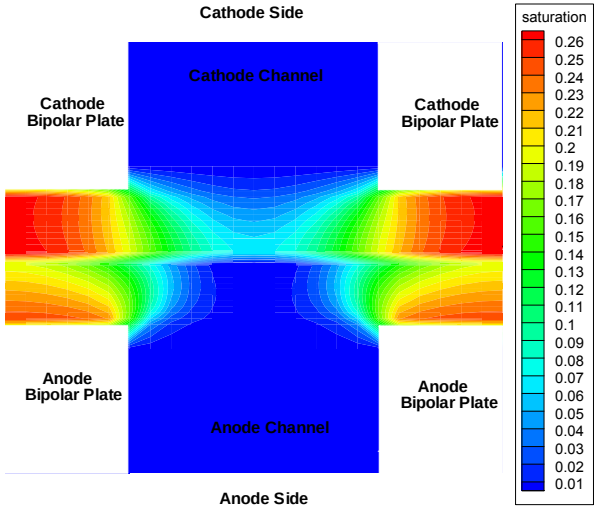

45% RH

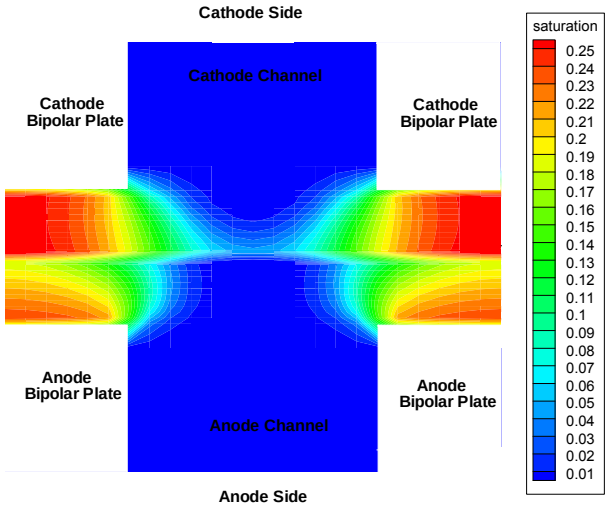

- **Liquid water diffuses across the GDL and it is transported away by liquid shearing through the channel.**
- **Liquid water tends to condense under the cooler land.**
- **The cathode side becomes drier as inlet humidity is reduced.**

Sandia National Laboratories

Effect of Inlet Humidity on Phase-Change Rate (I=1.0A/cm2, St=2.0, at Section B)

100% RH

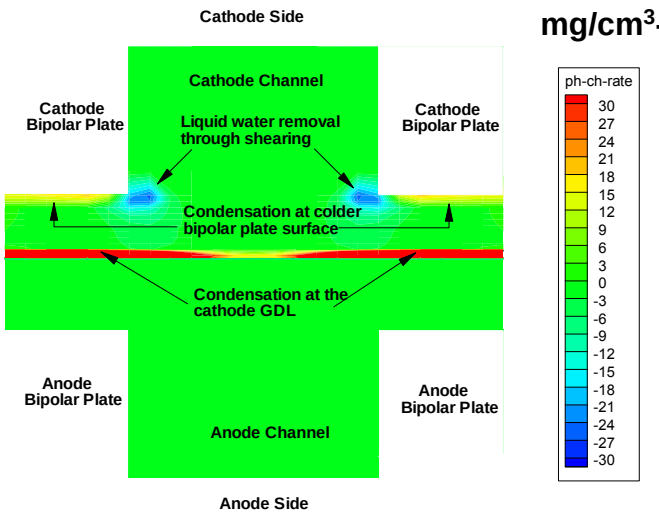

67% RH

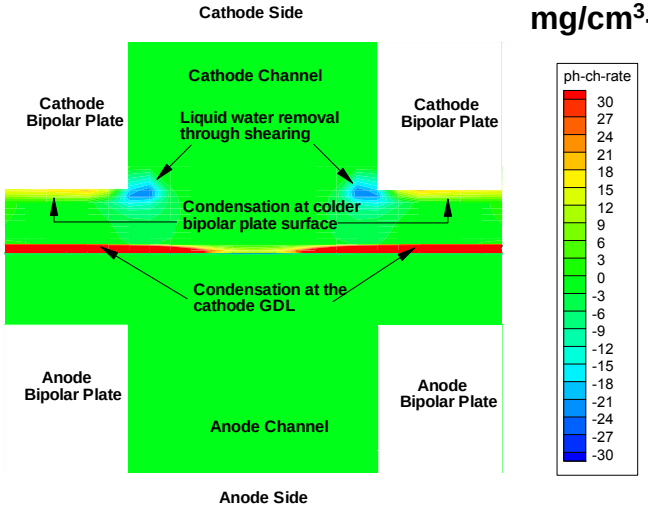

- **Water condenses on the cooler land surface.**
- **At the corner of land and channel liquid, shearing takes place in the channel.**
- **Condensation reduces as inlet humidity is lowered.**

45% RH

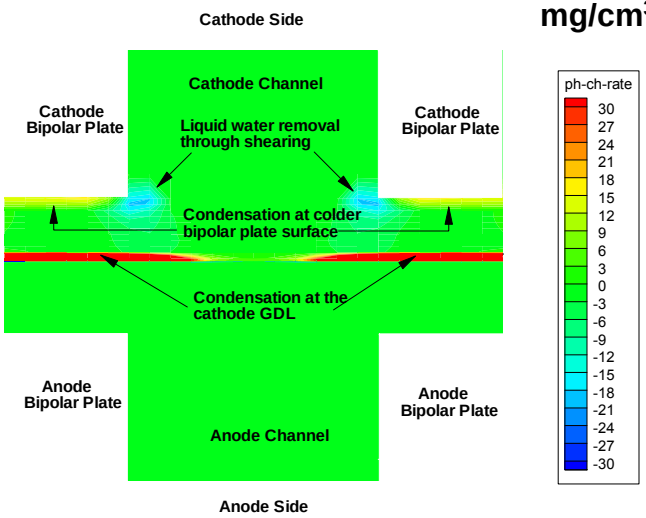

Effect of Inlet Humidity on Phase-Change Rate (I=1.0A/cm2, St=2.0, at Section B)

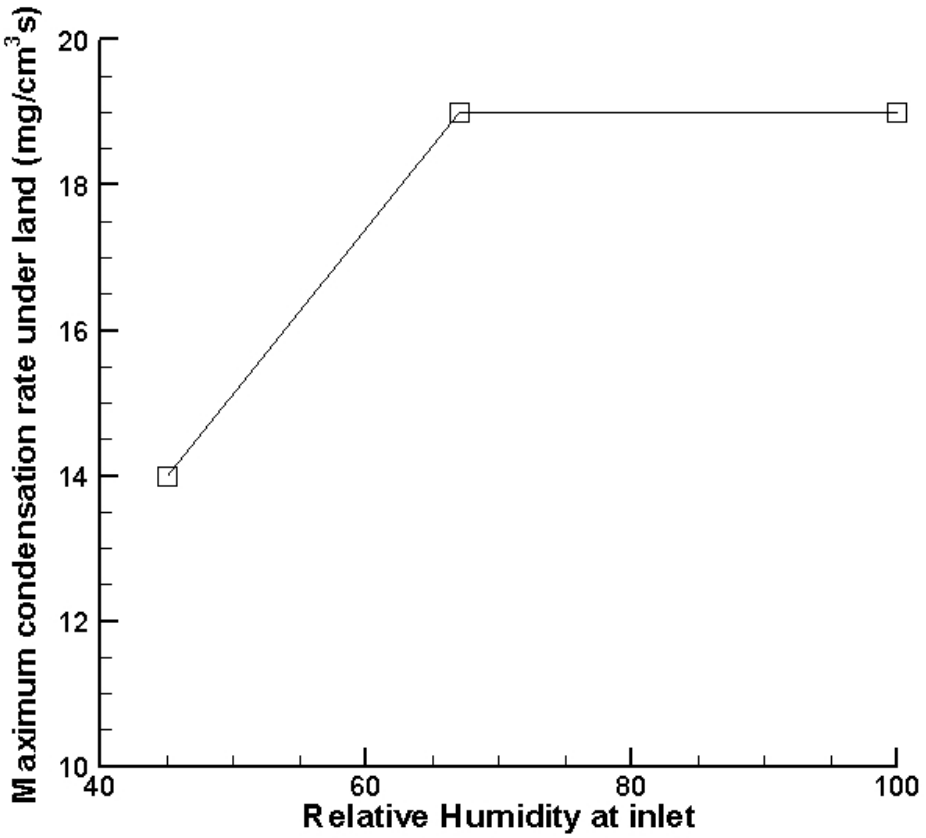

- **Maximum condensation rate levels out when %RH approaches ~ 67%.**
- **Rate of condensation drops as inlet humidity is lowered.**

Sandia National Laboratories

Summary

- **The key phenomena of liquid water transport and removal in PEM fuel cells were studied experimentally and computationally.**

– Observations from neutron radiography reveal liquid-water distribution within the active area of an operating fuel cell, and for the first time, liquid-water distribution across MEA.

– Data from direct optical visualization of water-droplet instability and detachment enabled the mapping of droplet instability diagrams.

– Simplified analytical models were developed to predict the droplet detachment in the low Reynolds number & inertia-dominating regimes and compared with experimental data.

– 3-D numerical model was developed and used to simulate the process of droplet detachment from the GDL/channel interface.

– Effect of microporous layer (MPL) on net water transport across membrane was studied numerically; cathode flooding can be reduced by making MPL more hydrophobic, increasing MPL thickness, and decreasing MPL mean pore size and mean porosity.

– Flow mal-distribution among PEM fuel cell channels was investigated numerically; high stoichiometric flow ratio can help flush liquid water from some PEMFC channels.

– Rate of phase change (condensation and evaporation) was computed using a 3-D two-phase model and the computed results help reveal where water vapor condenses and where liquid water evaporates. Condensation rate reduces as inlet humidity is lowered.